UNIVERSITY OF LJUBLJANA

Faculty of Mechanical Engineering

Observation of temperature fluctuations in the vicinity of vapour bubbles with microthermocouple device

Diploma thesis of the Erasmus+ Student Mobility for Studies programme

Mario Manjavacas Córdoba

Ljubljana, June 2023

UNIVERSITY OF LJUBLJANA

Faculty of Mechanical Engineering

Observation of temperature fluctuations in the vicinity of vapour bubbles with microthermocouple device

Diploma thesis of the Erasmus+ Student Mobility for Studies programme

Mario Manjavacas Córdoba

Mentor: Prof. Dr. Iztok Golobič
Co-mentor: Assist. Prof. Dr. Matevž Zupančič

Ljubljana, June 2023

University *of Ljubljana*
Faculty *of Mechanical Engineering*

Aškerčeva cesta 6
1000 Ljubljana, Slovenia
phone 00386 1 47 71 200
fax 00386 1 25 18 567
dekanat@fs.uni-lj.si

THESIS TOPIC APPLICATION

Erasmus+ Student: Mario Manjavacas Córdoba

Study Programme: Erasmus+ Student Mobility for Studies

Thesis topic for: Diploma Thesis

Number of the thesis topic: VS I/2007 E

Thesis topic title in English language: Observation of temperature fluctuations in the vicinity of vapor bubbles with microthermocouple device

Thesis topic title in Slovene language: Opazovanje temperaturnih nihanj v okolici parnih mehurčkov s pomočjo mikrotermočlena

Disposition of the thesis in English language:

Nucleate boiling is an extremely efficient convective heat transfer process, involving various heat transfer mechanisms. The contribution of individual mechanism can be studied based on the analysis of temperature fields of the boiling surface and temperature fluctuations within the working fluid itself. Since complete physical models for describing the complex boiling process are not yet available, an experimental approach is essential to obtain reliable temperature datasets.

In this diploma, first the existing literature on the topic of nucleate boiling should be presented, with a focus on the dynamics of vapor bubble formation and the influence of working fluid temperature near the boiling surface. Second, the experimental setup for nucleate boiling studies on thin metal substrates to allow in-liquid temperature measurement through a micro-thermocouple will be upgrade, and a measurement system for high-speed and high-resolution temperature measurements in the vicinity of vapor bubbles will be developed. Measurements of water nucleate boiling on a laser-structured nucleation site and obtain synchronized measurements using a video camera, an infrared camera, and a micro-thermocouple will be conducted. Finally, the temperature fluctuations of the working fluid during water boiling will be analysed and the results compared with existing data from the literature.

Note: Thesis must be submitted in linguistically and terminologically correct English language. The student must submit and defend his/her thesis during his/her study exchange at the Faculty of Mechanical Engineering, University of Ljubljana.

Disposition of the thesis in Slovene language:

Mehurčkasto vrenje je izredno učinkovit proces konvektivnega prenosa toplote, pri katerem nastopajo različni mehanizmi odvoda toplote. Doprinos posameznih mehanizmov je možno preučevati na podlagi analize temperaturnih polj vrelne površine in temperaturnih fluktuacij znotraj samega delovnega fluida. Ker popolnih fizikalnih modelov za popis kompleksnega procesa vrenja še ni na voljo, je za pridobivanje zanesljivih podatkov o temperaturah ključen eksperimentalni pristop.

Kandidat naj v delu predstavi pregled obstoječe literature na področju mehurčkastega vrenja s poudarkom na dinamiki tvorjenja parnih mehurčkov in vplivu temperature delovnega fluida blizu vrelne površine. Postavi naj eksperimentalno progo za preučevanje mehurčkastega vrenja na tankih kovinskih substratih nadgradite z možnostjo točkovnega merjenja temperature preko mikrotermočlena in zasnuje merilno verigo za hitretokoče in visokoločljivostno merjenje temperature v okolici parnih mehurčkov. Izvede naj meritve mehurčkastega vrenja vode na lasersko strukturiranem nukleacijskem mestu in pridobi sinhronizirane meritve s pomočjo video kamere, infrardeče kamere in mikrotermočlena. Na koncu naj analizira temperaturna nihanja delovnega fluida pri vrenju vode in rezultate primerja z obstoječimi podatki iz literature.

Mentor: Prof. Dr. Iztok Golobič

Co-mentor: Assist. Prof. Dr. Matevž Zupančič

Date of topic approval: 4. 5. 2023

UNIVERZA V LJUBLJANI
Fakulteta za strojništvo
14
Ljubljana

Note: Thesis must be submitted in linguistically and terminologically correct English language. The student must submit and defend his/her thesis during his/her study exchange at the Faculty of Mechanical Engineering, University of Ljubljana.

Acknowledgments

First, I would like to express my gratitude to mentor Prof. Dr. Iztok Golobič and co-mentor Assist. Prof. Dr. Matevž Zupančič for their guidance and help in the preparation of the final thesis. Without their help and attention, this work would not have looked as it does today.

I would like to express my heartfelt thanks for the help provided by the members of the thermal engineering laboratory. Especially Mattia Bucci, who has guided, advised, and always taught me the necessary knowledge for my thesis. I also appreciate his time helping me to understand the theoretical background applied to the experiments performed and their results.

Finally, I would like to thank my family for their support, motivation and advice that helped me to overcome the times when I needed the encouragement.

Declaration

1. I, the undersigned Mario Manjavacas Córdoba, born 23 November 2001 in Spain, Erasmus+ student at the Faculty of Mechanical Engineering at the University of Ljubljana, hereby declare that this undergraduate thesis titled *Observation of temperature fluctuations in the vicinity of vapour bubbles with microthermocouple device* is my own original work created under the supervision of my advisor Prof. Dr. Iztok Golobič and co-advisor Assist. Prof. Dr. Matevž Zupančič.

2. I hereby declare that the submitted electronic copy of this undergraduate thesis is identical to the printed copy.

3. Pursuant to the provisions of the Copyright and Related Rights Act (Official Gazette of the Republic of Slovenia, No. 21/1995 as amended), I hereby expressly give my permission for this undergraduate thesis to be published on the websites of the Faculty of Mechanical Engineering and the University of Ljubljana.

4. By signing this Declaration, I grant my permission for this undergraduate thesis to be made publicly accessible online via the Repository of the University of Ljubljana.

By signing this document, I certify that:
- the presented text is the product of my own original research in its entirety;
- the presented text adheres to linguistic and stylistic conventions and the technical requirements of the Guidelines for Composing Final Theses, meaning that:
  - the works and opinions of other authors used in this undergraduate thesis are appropriately cited or acknowledged pursuant to the Guidelines for Composing Final Theses, and
  - I have obtained the permission for the use of any data and original work reproduced in the text in full (either as text or as a graphic) from their respective authors and duly noted that in the text itself;
- I am aware that plagiarism, i.e. the misrepresentation of someone else's work (be it text or graphics) as my own, is a crime under the Criminal Code of the Republic of Slovenia (Official Gazette of the Republic of Slovenia, No. 55/2008 as amended);
- I am aware of the potential repercussions concerning my status at the Faculty of Mechanical Engineering at the University of Ljubljana as per the applicable Rules should plagiarism be proven in connection to the submitted undergraduate thesis.

Ljubljana, 19th June 2023 Signature of the author:

Abstract

UDC 536.2:536.532:66.046.7(043.2)

No.: VS I/2007 E

Observation of temperature fluctuations in the vicinity of vapour bubbles with microthermocouple device

Mario Manjavacas Córdoba

Keywords: nucleate boiling
microthermocouples
seebeck effect
high-resolution measurements
thermal boundary layer

Nucleate boiling is an effective heat transfer process important in many engineering applications and is mostly evaluated through experimentally obtained data, since modelling is challenging due to the complexity of the process. In this context, obtaining information about the transient temperatures on the surface and in the liquid can help us understand individual contributing mechanisms of bubble growth. While the infrared thermography is reliable approach to measure transient temperature fields at the boiling surface, the in-liquid measurement methods are still underdeveloped. Therefore, this thesis focuses on development and implementation of microthermocouple device that is used for high spatiotemporal resolution temperature measurements in the vicinity of growing vapour bubble during atmospheric boiling of water. Moreover, microthermocouple was implemented into existing boiling setup with synchronized high-speed infrared thermography and video camera. Results consist of static calibration procedure, measurement of microthermocouple's dynamic response, determination of thermal boundary layer formation under rapid heat input and measurement of temperature in liquid and vapor during bubble growth on laser-textured nucleation site. It is shown that developed methodology has an excellent potential of providing additional dimension on the dataset, needed for evaluation of local heat fluxes at vapor-liquid interface that are currently not well understood.

Izvleček

UDK 536.2:536.532:66.046.7(043.2)

Tek. štev.: VS I/2007 E

Opazovanje temperaturnih nihanj v okolici parnih mehurčkov s pomočjo mikrotermočlena

Mario Manjavacas Córdoba

Ključne besede: mehurčkasto vrenje
mikrotermočleni
seebeckov efekt
visokoločljivostne meritve
termična mejna plast

Mehurčkasto vrenje je učinkovit način prenosa toplote, pomemben v številnih inženirskih aplikacijah. Parametre vrenja se večinoma določa z eksperimentalnim pristopom, saj je modeliranje zahtevno zaradi kompleksnosti samega procesa. Pri tem so pristopi za določanje temperatur na vrelni površini in v fluidu posebej pomembni, ker omogočajo pridobitev podatkov za analizo nastopajočih mehanizmov v različnih fazah nastanka mehurčkov. Čeprav je infrardeča termografija uveljavljena za meritve nestacionarnih temperaturnih polj na površinah, so metode za visokoločljivostno merjenje temperatur v fluidu med vrenjem nezadostno razvite. Obstoječa naloga naslavlja to vprašanje preko implementacije mikrotermočlena v obstoječi eksperimentalni sistem, ki vključuje tudi sinhrono spremljanje temperatur površine preko hitrotekoče infrardeče termografije in vizualizacijo rasti mehurčkov preko hitrotekoče video kamere. Ugotovljeno je, da je razviti mikrotermočlen sposoben zajemati visokoločljivostne podatke predvsem v časovni domeni zaradi majhne termične časovne konstante. Rezultati so prikazani za statični kalibracijski test, dinamični odziv mikrotermočlena, razvoj termične mejne plasti nad grelno površino ter meritvijo temperature v kapljevini in pari med rastjo parnih mehurčkov na lasersko strukturiranem nukleacijskem mestu. Ugotavljamo, da ima razvita metodologija velik potencial za pridobivanje do sedaj še nepoznanih eksperimentalnih podatkov, ki so potrebni za določitev lokalnih toplotnih tokov predvsem na meji med kapljevino in paro, kar do danes še ni ustrezno pojasnjeno.

List of contents

List of figures

List of tables

List of symbols used

Symbol	Unit	Meaning
A	m^2	area
D	mm	diameter
f	Hz	frequency
R	mm	radius
S	μV/°C	Seebeck coefficient
t	s	time
T	ºC	temperature
U	V	voltage
$\dot{q}$	kW/m^2	heat flux
ΔT	K	temperature difference
ΔU	V	voltage difference
θ	º	contact angle
τ	s	time constant
ρ	kg/m^3	density
γ	N/m	surface tension

Indexes	
adv	advancing
b	bubble
d	departure
f	footprint
g	growth
L	liquid
LV	liquid-vapor
m	measured
ref	reference
rec	receding
sat	saturation
static	static
V	vapor
w	wait

List of abbreviations used

Abbreviation	Meaning
ADC	Analog to digital converter
EMF	Electromagnetic force
IR	Infrared
MTC	Microthermocouple
TBL	Thermal boundary layer

1 Introduction

1.1 Background of the problem

Nucleate boiling is highly efficient heat transfer mechanism utilized in many engineering fields like cooling of nuclear fuel claddings, microelectronics, concentrated solar systems and even propulsion systems in space applications. During nucleate boiling, vapor bubbles are produced on the heated surface, which removes significant amount of energy due to the large latent heat of the working fluid, as specially when using water. Growth of vapor bubbles results in transient temperature fields that are created on the heated surface and inside the liquid as well. In this context, temperature measurement is essential to comprehensively investigate boiling performance, boiling mechanism and finally to fully understand the process for further optimization requirements.

There are several methods to measure transient temperatures during the boiling process. Detecting transient temperature fields on the heated surface is mostly performed with high-speed infrared (IR) thermography, but researchers also demonstrated other techniques like temperature sensitive paints, fluorescence thermometry and array of miniature temperature sensors. Measurement of transient temperature inside the liquid and inside the vapor bubble is however more challenging. There have been several attempts to accurately detect temperature around a vapor bubble via schlieren effect, phase-shift interferometry and two-color laser-induced fluorescence. Despite the great efforts and advance measurement equipment, those techniques showed disadvantages connected with large uncertainties and insufficient temporal or spatial resolution. For that reason, in-liquid measurement with miniature thermocouples and adequate data acquisition is still and interesting classical alternative to investigate boiling phenomena.

1.2 Objectives and research hypothesis

The main objective of this diploma is to set up a framework to allow in-liquid temperature measurement through a micro-thermocouple device during a boiling process, where the entire system should be coupled with a high-speed video camera and high-speed IR thermography. To achieve this goal, we aim to develop a custom-made microthermocouple, set up a measurement chain and perform calibration procedure by utilizing high-speed 24-bit data acquisition system and finally upgrade the existing boiling chamber with a

microthermocouple and conduct controlled boiling experiment to provide a new datasets for future studies of complex heat transfer mechanisms during boiling. Additional objective is to provide adequate literature review of thermocouple measurement principles and bubble dynamics to point our most important current knowledge gaps in this field.

Finally, or work is focusing on the following research hypothesis:

- Custom-developed microthermocouple device, comprised or the bimetal wire of 25-μm thickness, can be successfully used to measure the transient temperatures in the vicinity of nucleating bubbles during pool boiling of water with a spatial resolution of ~20 μm and a temporal resolution of ~1 ms.

2 Theoretical foundations and literature review

2.1 Concept of temperature measurements with thermocouple

2.1.1 Seebeck effect

The thermoelectric effect is the direct conversion of a temperature difference to electric potential and the other way round through a thermocouple, which is essentially a wire pair of two different materials and connected at both ends. The Seebeck effect is a physical manifestation of the thermoelectric effect, and it refers to the appearance of electric potential difference between a thermocouple when its ends are exposed to different temperatures. As the difference of temperature grows, a stronger electromotive force (EMF) is developed across both points with different temperature. Depending on the materials used, there is a different ratio between EMF and temperature difference. As this effect is proportional, it leads to the Seebeck coefficient, which is to be detailed later. These coefficients vary as function of temperature and depend on the composition of the used conductor material.

Peltier effect is the inverse of the Seebeck effect, where a difference in temperatures in both ends of the thermocouple is created when a voltage difference is applied between both terminals. Some literature refer to this whole process as the Peltier-Seebeck effect although only the Seebeck will be of interest in this work, since it will lead to the thermocouples that will be developed. In this paper, Seebeck effect manifestation will be used as a tool to measure temperature through thermocouples.

A thermocouple is a sensor made of two metals used to measure temperature thanks to the Seebeck effect. When the junction of the metals is heated, a voltage difference is produced, which is what allows us to know the temperature. However, depending on the range of measurements they can carry out and the environment in which they can work, they can be classified into different types. To characterize them, it is important to know the temperature range in which each type of thermocouple can work and, on the other hand, the Seebeck coefficient they have. This coefficient indicates the voltage induced in response to a

temperature difference. The higher the Seebeck coefficient, the better it can detect small temperature variations, which can be an advantage.

The most used are the J, K and T types [1]:

- Type J thermocouple is made of iron/constantan (copper-nickel) metal pair. It is notable for measuring temperatures between 0 and 760˚C as well as for its low cost. However, the maximum temperature at which it can measure depends on the wire gauge, i.e. the wire diameter. These thermocouples have a notable application in the plastics industry as they are frequently used to monitor the temperature of injection molding machines. On the other hand, they have a Seebeck coefficient of 51 μV/˚C. Their main problem is the oxidation that iron can undergo above 550˚C.
- T-type thermocouple: is composed of copper/constantan. Its temperature range is between -200 and 371˚C, above which oxidation on copper increases. It is particularly useful for use at low temperatures. Its coefficient is 40 μV/˚C.
- Type K thermocouple is composed of chromium/alumel. It is notable for its wide temperature range from -200 to 1260˚C. This characteristic, together with the fact that it is a very economical type of thermocouple, makes it the most widely used. It is also noted for its good resistance to corrosion. Its sensitivity is 40 μV/˚C. Although it is the most generic thermocouple, it is also used in nuclear applications.

It should be noted that our thesis is focusing on using a microthermocouples, developed o a ultra-thin wire gauge with a typical diameters of 50 μm or less. Despite that, the working principle is exactly the same as with normal gauge thermocouples, the main difference is their fragility and susceptance to pick up noise during measurement, which will be discussed later. Regardless of the thermocouple type and diameter, one always needs an accurately determined Seebeck coefficient to calculate temperatures based on a reading of voltage using the following equation:

$$\Delta V = S \cdot \Delta T \ , \tag{2.1}$$

where S is the Seebeck coefficient or sensitivity of the thermocouple, ΔV the voltage difference and ΔT the temperature difference measured between both ends of the thermocouple. In this case, the temperature difference can be defined as:

$$\Delta T = T_{\mathrm{m}} - T_{\mathrm{ref}} \ , \tag{2.2}$$

where T_{m} is the measured value and T_{ref} is the reference value, further explained in the next chapter and through the Figure 2.1. That said, to accurately measure the absolute temperature via thermocouple, one need and information about the reference temperature point. This value should be obtained by some external and additional temperature measurement device or by exploiting a well-known temperature point – for example a mixture of pure water and ice at atmospheric pressure, which gives 0 °C reference.

2.1.2 Data acquisition system for thermocouple measurements

In this work, type K thermocouple will be used and demonstrated, since it can provide high sensitivity, a wide measurement temperature range and it is also highly resistant to corrosion. There are two ways of measuring temperatures with the aim of thermocouples, depending on the way of measuring reference temperatures. In the first one, as shown on Figure 2.1, a cold bath for the temperature reference is needed, where one end of the thermocouple will be usually submerged at 0°C. Assuming a Seebeck coefficient of 40 μV/˚C, the equation that will be used can be written as:

$$\Delta V = S \cdot \Delta T = S \cdot \left(T_m - T_{ref}\right) = 40 \cdot (T_m - 0) = 40 \cdot T_m \qquad (2.3)$$

Thus, knowing the voltage difference (in μV) and clearing the 40μV/˚C from the equation, the temperature T_m can be obtained.

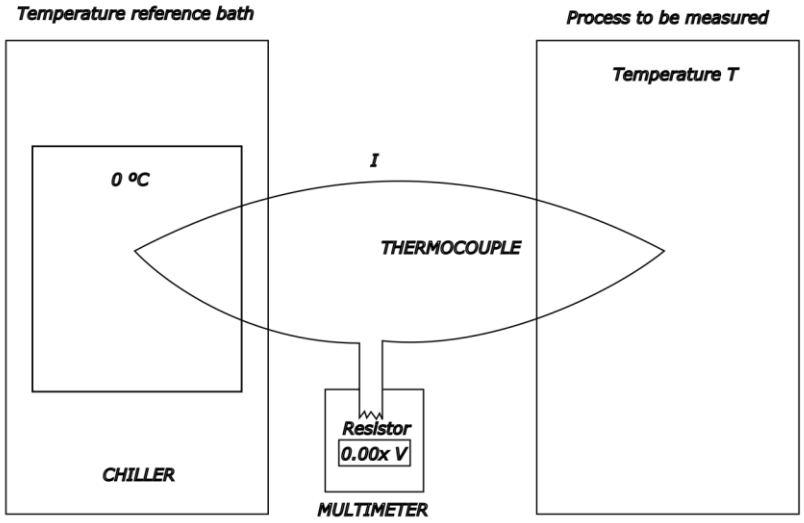

Figure 2.1: Basic schematic data acquisition system for thermocouple temperature measurement.

Apart from this method, there exists an advanced and more straight forward way to perform these measurements without the need for a thermostatic bath, as shown in Figure 2.2. This way, measurement devices can be smaller and more portable. Although this is not the method that will be used for this work, it deserves quite a mention, since it is the most used in real industry. This kind of devices are a kind of multimeters that are already prepared for temperature measurements with thermocouples. They have a thermocouple cable input and they are equipped with a thermistor inside. A thermistor has a variable resistance dependent on temperature. These resistors are calibrated so the multimeter can acquire the reference temperature, which is usually about to be ambient temperature around 20ºC, and compensate the reading. These devices usually can give T_m directly, instead of the voltage reading, so the user doesn't need to calculate for each value. The disadvantage of this measuring principle is relatively slow response (usually < 10 ms) and relatively high absolute measurement uncertainty (usually > 0,5 K) due to intrinsic uncertainty of the thermistor.

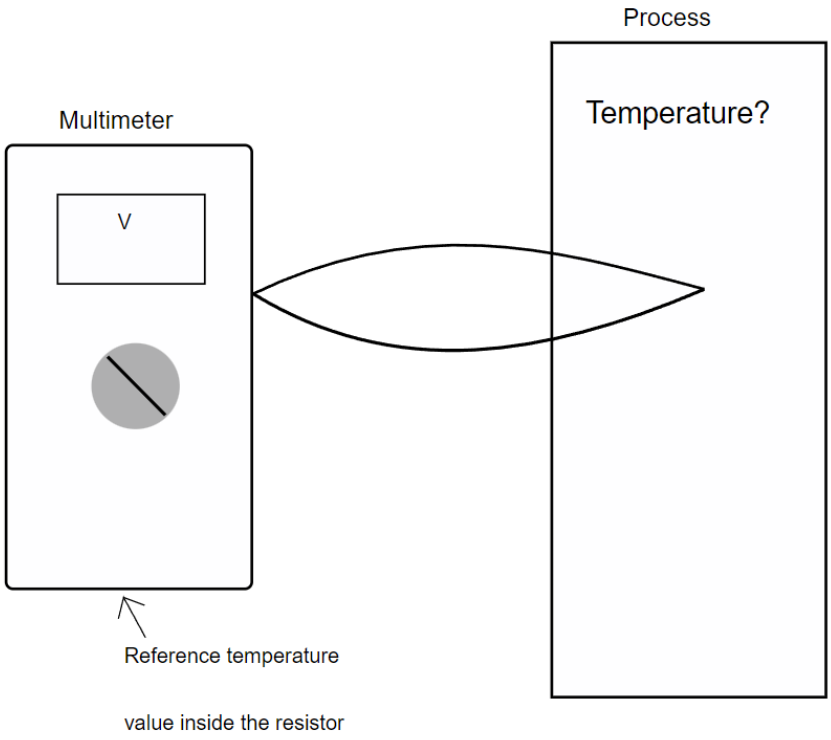

Figure 2.2: Schematic data acquisition system with a multimeter with built-in thermistor.

2.2 Temperature measurement in nucleate boiling process

Nucleate boiling has been an important area of research in liquid vapor heat transfer over the past century [2], with the aim of improving the boiling process by reducing surface temperature and increasing the critical heat flux. However, due to the complexity of the boiling process, a definitive physical model has not yet been established, making experimental research necessary.

Pool boiling is a process where a seemingly stationary pool of liquid is placed atop the heated surface, where the surface is heated above the liquid's saturation temperature until the vapor bubbles are generated. As presented in Figure 2.3, there are different types of boiling regimes depending on the temperature of the heated surface and resulting vapor formations. If the surface superheat is small, the heat is only removed via natural convection without any vapor formation, but at higher superheats the onset of boiling appears and bubbles form on the surface and remove heat from it through a combination of evaporation (involving latent heat) and convective heat transfer. As the heat flux increases, bubble coalescence increases until it reaches a critical point known as the critical heat flux, beyond which the heat transfer coefficient drops sharply. If the heat flux is further increased, the system enters the film boiling regime that usually destroys the surface due to extremely high temperatures that take place at this point.

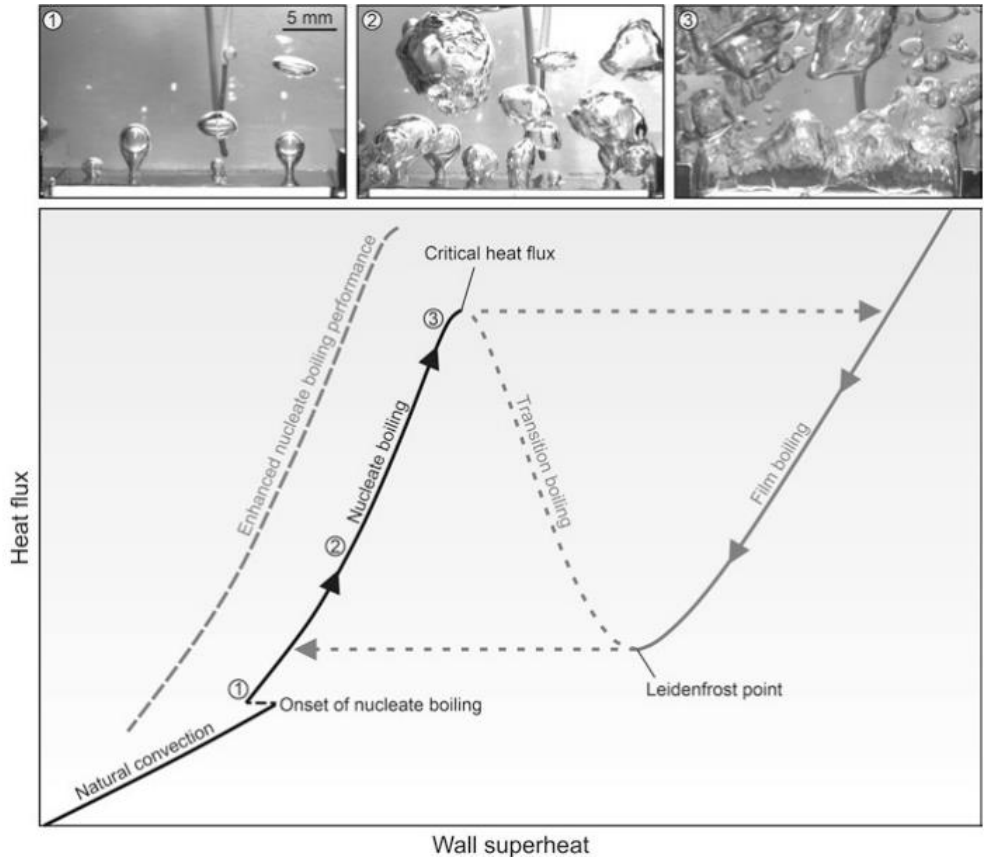

Figure 2.3: Boiling curve and nucleate boiling regimes. [2]

Nucleate boiling is affected by various factors such as surface characteristics, fluid properties, surface-fluid interactions, and operating conditions. To enhance the boiling process, the surface can be modified to achieve a lower surface temperature at the onset of boiling, increase the density of nucleation sites, limit bubble growth, and delay dry-out.

Functionalizing the boiling surface can be achieved by creating (super)hygrophobic or (super)hygrophilic surfaces. The former prefer the vapor phase and promote nucleation activation, while the latter delay the critical heat flux but increase surface superheat at low heat fluxes. These surface characteristics significantly impact key boiling heat transfer parameters. Overall, finding the ultimate approach for enhancing boiling is a challenging task, but modifying surface properties is a promising area of research. It is still unknown, however, how functionalized surfaces affect the temperature field distribution around the vapor bubbles and if the also affect the formation of thermal boundary layer (TBL) that forms prior to vapor nucleation. These knowledge gaps could be addressed through the appropriate measurement techniques. However, to enhance the overall boiling performance, one needs to first investigate the complexity of boiling on a single bubble event, further explained in the following chapter.

2.2.1 Bubble life cycle

In boiling, each vapor bubble undergoes several significant stages, namely the nucleation, growth and departure, followed by a waiting time prior to the next nucleation event [3].

Bubble nucleation is the initial stage of the bubble cycle. To start bubble formation in a liquid, it requires the existence of a vapor embryo, which can be formed by homogeneous or heterogeneous nucleation. The fundamental distinction between homogeneous and heterogeneous nucleation lies in their location relative to the surface of the system. Homogeneous nucleation takes place in regions far from the surface, while heterogeneous nucleation occurs directly at the surface. In other words, in homogeneous nucleation, thermal fluctuations of the liquid molecules trigger vapor core formation in areas distant from the surface, whereas in heterogeneous nucleation, vapor core formation occurs specifically at the surface of the system itself. This works particularly focuses on heterogenous nucleation events.

Bubble nucleation involves the trapping of air bubbles in cavities on a surface generating nucleation cores. This can be explained thanks to the entrapped vapor theory [4] proposes that the trapped bubbles have a convex curvature, resulting in higher vapor pressure inside the bubble compared to the surrounding liquid. When the liquid is superheated, its equilibrium vapor pressure becomes greater than that inside the bubble, leading to the growth of the bubble [5].

Sequentially in the bubble cycle, the bubble starts to grow, leading to the next phase. The growth of the bubble is influenced by the wetting behavior as well as the difference in temperature between the bubble and the surrounding liquid or, as it was called previously, the superheat [5]. Cooper and Lloyd's study [6] explains the process of bubble growth in pool boiling. Their study consists in the phenomenological model. This model explains that the bubble grows as a result of the evaporating superheated liquid surrounding it and the microlayer located under the bubble. In Figure 2.4 the different steps in heat transfer during the bubble growth are explained [7].

As the bubble grows, it displaces the surrounding liquid and leaves a thin liquid film, known as the microlayer, on the heated wall [Figure 2.4(a)]. Then, the microlayer evaporation occurs rapidly due to its low thermal resistance, leading to dry-out and the spread of a dry-patch from the center [Figure 2.4(b)]). During the bubble departure process, which will be explained later, the contact area decreases at the same time the bubble grows longitudinally, causing the rewetting of the dry-out area by the liquid flowing beneath the bubble while is departing [Figure 2.4(c)]). Once the bubble has departed due to buoyancy, the flow of liquid follows its path due to partial flow entrainment and the nucleation point is covered by liquid, which is frequently denoted as quenching, shown in Figure 2.4(d).

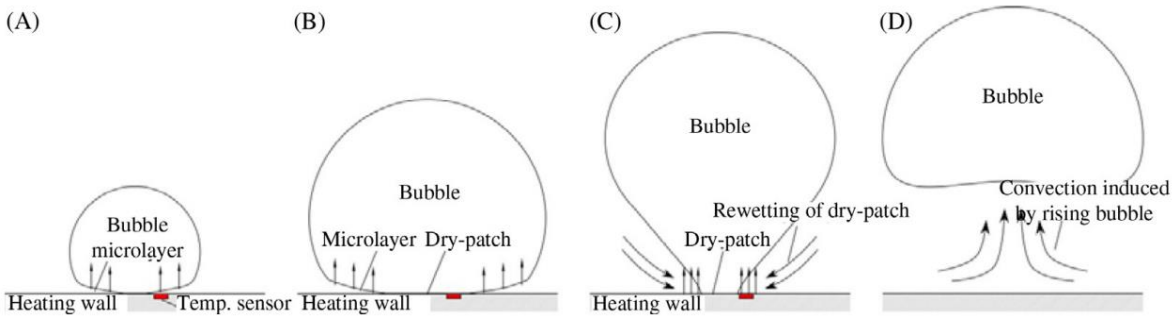

Figure 2.4: Fundamental heat transfer phenomena under an isolated boiling bubble. [7]

The bubble growth cycle repeats at a certain frequency. Previous studies from Mikic et al. have shown that bubble growth can follow two regimes [8]. First one is present at short timescales, where the growth is dominated by inertia and can be described by the Rayleigh equation, saying that bubble radius (R_b) is increasing proportionally with time ($R_b \propto t$). On the other hand, at longer timescales, growth is limited by heat diffusion, and the Plesset and Zwick's description shows that $R_b \propto t^{1/2}$ [9]. It has been observed that the transition from inertia-dominated to diffusion-limited growth occurs in less than one millisecond. Since time departure of a bubble is normally tens of milliseconds, it is assumed that growth is described by the second regime, limited by heat diffusion. Although these two studies, the Mikic's and Plesset and Zwick's studies, did not consider the contribution of microlayer evaporation, van Stralen et al. study showed that microlayer growth also follows a similar pattern with a $R_b \propto t^{1/2}$ dependence [10]. Analyzing the growth of bubbles using Mikic's model, it can be seen in
Figure 2.5 how the equivalent bubble radius (R_b), which was calculated using the bubble volume, changes trough time in different wall superheat conditions.

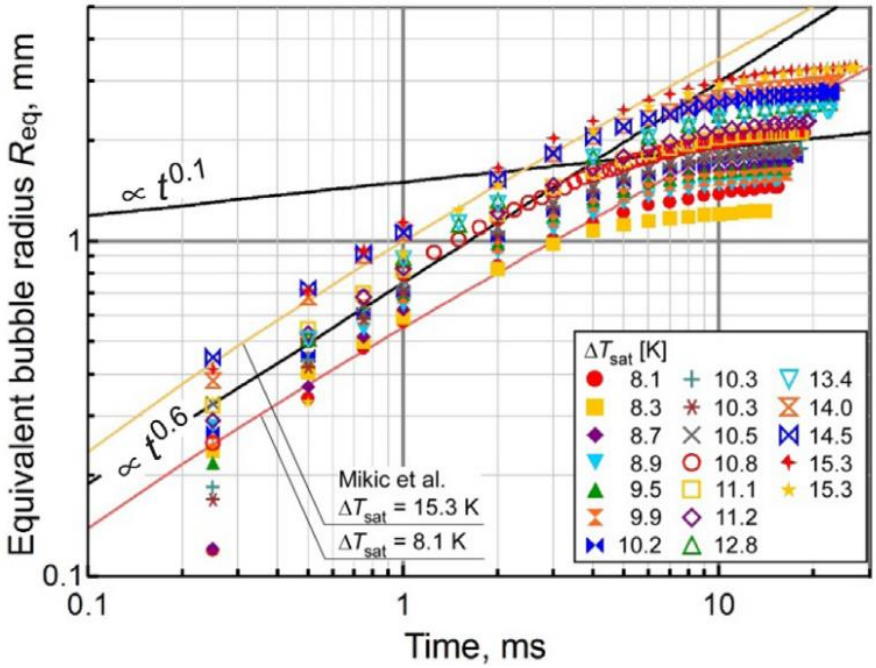

Figure 2.5: Bubble growth in isolated pool boiling of water (ΔT_{sat} = 8–15 K, R_{max} = 1.2-3.6 mm). [7]

As the Figure 2.5 indicates, the experimental results demonstrate that the bubble growth relation is proportional with time to the power of 0.6 until 3–5 milliseconds after nucleation began. Then the growth has a relation proportional with time to the power of 0.1. This growth behavior in the early to middle stages, proportional with time to the power of 0.6, is perfectly described by Mikic et al.'s model, which considered the thermal diffusion and liquid inertia in the semi-infinite superheated liquid surrounding the bubble. Otherwise, in the middle to final stages, the bubble growth slows down due to the consumption of enthalpy in the superheated liquid surrounding the bubble. The exact behavior and contribution of superheated layer around the bubble could be further explained through understanding and experimental data about the temperature field around the bubble. This data is currently lacking in the present literature and is partially addressed within our work.

The last phase in bubble life cycle is the departure, where bubbles tend to rise away from the boiling surface. This occurs due to the combined influence of several forces, including buoyancy, momentum, and surface tension. However, in most cases where bubbles form at a solid surface, the way the surface interacts with the liquid, known as wettability, determines how the bubbles look as they form, grow and depart. In simpler terms, the bubbles rise up and detach from the boiling surface because of a complex interplay of different physical forces and the interaction between the surface and the liquid [5], [11].

In order to predict or at least understand when the bubble will depart, first, the concept of contact angle has to be explained. There are three types of contact angle depending on the interaction between the fluid and the surface which are static (θ_{estatic}), advancing (θ_{adv}) and receding (θ_{rec}) as it is shown in Figure 2.6. When boiling experiments come to practice, the bubbles form, grow and departure mostly at the same place in an horizontal flat surface, thus the static contact angle (θ_{estatic}) is the most frequently metric used for wettability in boiling studies. It is important to understand that the static contact angle may not always accurately represent the equilibrium contact angle especially if there is a significant difference between the advancing and receding contact angles, where the static contact angle is result of an angle between these two contact angles [11].

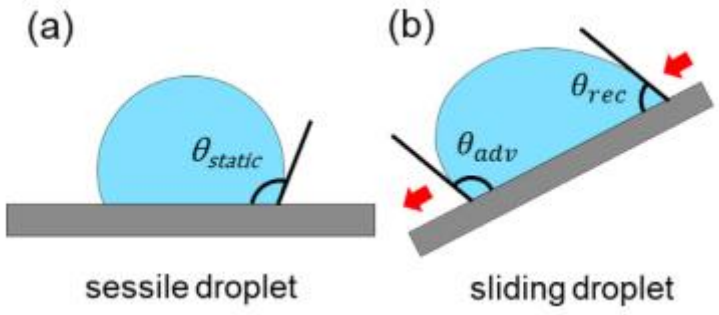

Figure 2.6: Illustration of (a) static and (b) dynamic contact angles. [11]

Fritz was the pioneer in establishing a correlation between the bubble departure radius, and the static contact angle by means of a balance between buoyancy force and surface tension force as shown in Figure 2.7. The proposed correlation is expressed by the following equation:

$$R_d = 0.0104 \times \theta_{static} \times \sqrt{\frac{\gamma_{LV}}{g(\rho_L - \rho_V)}}, \tag{2.4}$$

where g denotes the gravitational acceleration, θ_{static} represents the static contact angle in degrees, ρ is the density of liquid (index L) and vapor (index V) and $\gamma_{\text{L}}$is the surface tension between liquid and vapor.

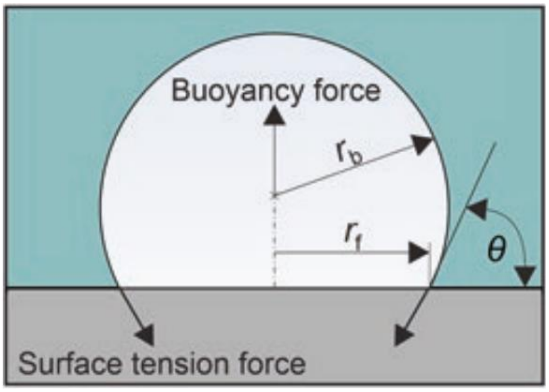

Figure 2.7: Illustration of buoyancy and surface tension forces acting on a growing bubble. [2]

Later on, Phan et al. [12] took a different approach to the situation. Instead of focusing on the balance between buoyancy force and surface tension, they analyzed the comparison of two spherical bubbles with different contact angles, but the same footprint as seen in Figure 2.8.

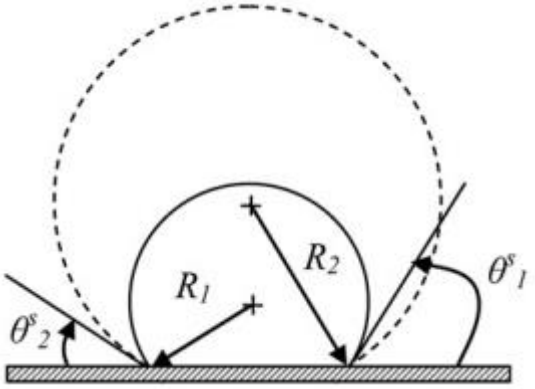

Figure 2.8: Two spherical bubbles are assumed to have the same triple contact line (TCL) and different static contact angles. [12]

Interestingly, they found that the bubble with a larger contact angle would always be larger due to simple geometrical reasons related with the contact angles. To address this finding, they modified the model proposed by Fritz by considering the energy factor $f(\theta)$, which is necessary for the formation of a bubble. As a result of this analysis, a new bubble departure radius correlation was proposed:

$$R_d = 0.626977 \times \frac{2 + 3\cos\theta - \cos^3\theta}{8} \times \sqrt{\frac{\gamma_{LV}}{g(\rho_L - \rho_V)}} \tag{2.5}$$

Despite numerous studies, it has not yet been possible to develop a universal model to accurately predict bubble size and bubble growth time for a wide variety of applications. This is due to several reasons related to accurate wettability determination, but most of all also related to the unknown contribution of the heat flux that powers the bubble growth from

the heated surfaces via microlayer evaporation and from the superheated liquid around the bubble.

To conclude, having explained all the processes that a bubble goes through from the nucleation to the departure, we can continue to explain how the surface temperature fluctuates during the bubble growth through the Figure 2.9. Firstly, the nucleation occurs (stage 1). The onset of nucleation is evidenced by an abrupt decrease in temperature together with a high localized heat flux, which is accompanied by an increase in both the bubble radius and the size of the bubble footprint.. At second stage the bubble grows and at some point the bubble radius keeps increasing, but the bubble footprint decreases. As the buoyancy force begins to lift the bubble from the surface, the bubble footprint decreases until finally the bubble detaches. This is happening during the stage 3, when the bubble departs, and the bubble footprint decreases until reaching zero. After stage 3 the wall temperature increases trough time. The period from the begining of nucleation to detachment is known as the bubble growth time (t_g). After the bubble detaches, a thermal boundary layer forms again while the cold liquid wets the nucleation site. This period is called the waiting time (t_w), and lasts until the next nucleation occurs. The sum of the growth time and the waiting time is the total period (t_b), which is inversely proportional to the nucleation frequency ($f_b = 1/t_b$) [2].

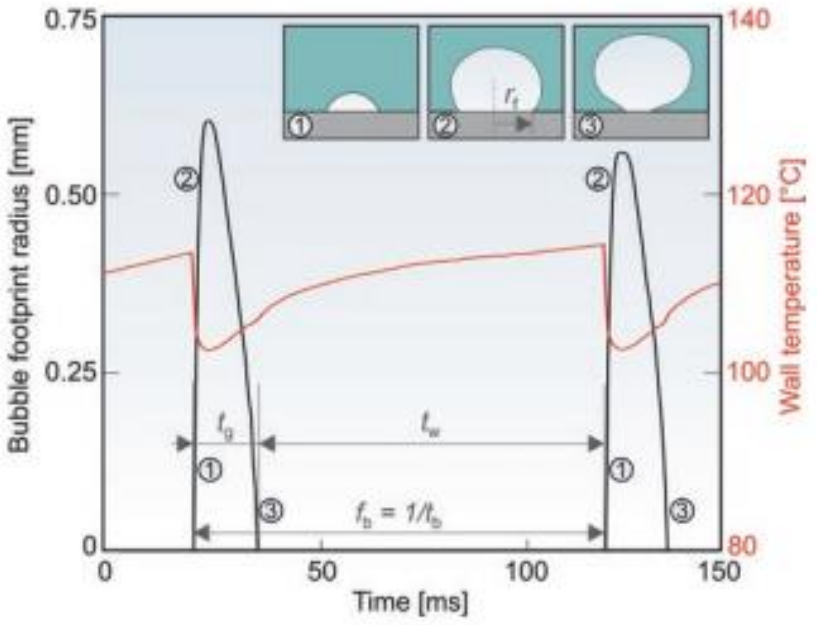

Figure 2.9: Wall temperature and the bubble's footprint radius development during the bubble life cycle. [2]

2.2.2 Usage of microthermocouples in boiling research

To better understand the boiling process at the microscopic level and to answer the knowledge gaps pointed out in the previous chapters, microthermocouples were already used by several researches. These miniaturized sensors allow precise measurement of temperature fluctuations during the formation and growth of bubbles in liquids. Microthermocouples (MTC) provide valuable information to improve theoretical models, optimize heat exchangers and other heat transfer devices, allow optimization in cooling application, and advance the understanding of boiling.

M. Buchholz et al. [13] aimed to develop a device to obtain accurate measurements in terms of spatial and temporal dimensions to investigate temperature fluctuations on a heated surface. For that purpose, special array micro-thermocouples have been developed. In their investigation, they used several microthermocouples with a diameter of 38 μm and placed at a depth of 3.6 μm below the surface of the heater. In total, 36 MTCs are arranged in an area of 1 mm², with 8 additional MTC surrounding this field, as it is shown in Figure 2.10.

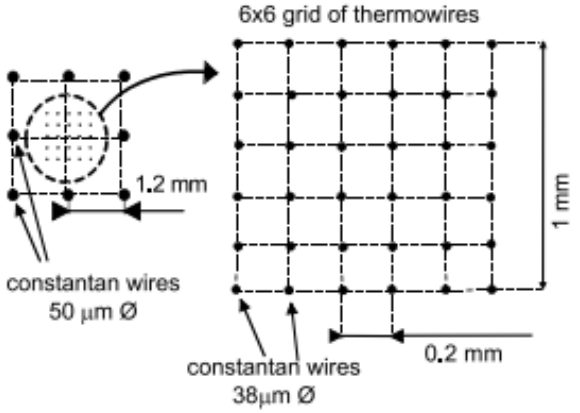

Figure 2.10: Designed positions of microthermocouples. [13]

They proved that with increasing wall superheat, the temperature fluctuations on the wall also increases to a certain level, as it is shown in Figure 2.11. Interestingly, when reaching the film boiling regime, the temperature fluctuations stop to exist, as the surface is not wetted any more. On the other hand, in nucleated boiling, critical heat flux (CHF) and transition boiling, there is existence of steep temperature drops, but on a different time scales mainly due to different bubble coalescence behavior during different stages.

During nucleated boiling, the presence of continuous nucleation and the growth of a bubble at the MTC junction is observed. In transition boiling, a temperature drop can be interpreted as a rewetting of the surface, followed by nucleation and growth of small bubbles. This is due to the intermittent existence of unstable vapour patches on the surface. Even more, under conditions of low heat flux (high superheat) in the transition boiling, there is no liquid-rich layer on the heater surface. During transition boiling, the transient temperature can experience rapid increases of up to 10,000 K/s during a period of rewetting. In summary, M. Buchholz [13] and his colleges demonstrated that MTCs are a specialized measurement technology that allows detailed analysis of temperature fluctuations and boiling properties in a heated surface. Their precise layout and small size make them ideal for obtaining accurate data on surface wetting and bubble nucleation.

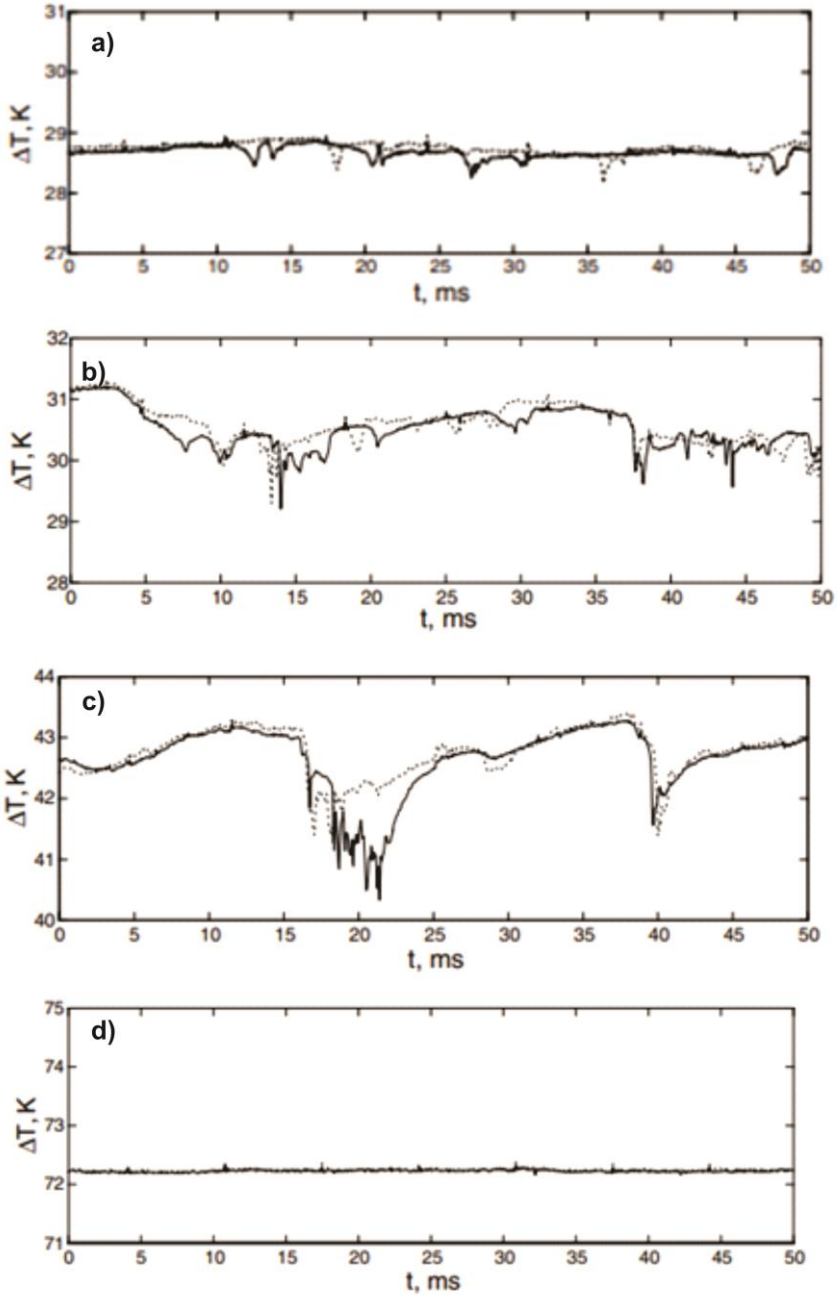

Figure 2.11: Results of measurements through array of MTCs for (a) nucleate boiling regime, (b) near CHF regime, (d) transition boiling and (d) film boiling. [13]

In a different study, A. Ono and H. Sakashita [14] investigated how vapour masses behave under high heat flux conditions. In their experiment they measured in-liquid temperature with MTC in relation to different distances to the heating surface. They proved that different temperature patterns were observed depending on the measuring height as shown in Figure 2.12. At first, at a considerable distance from the heating surface of 12.253 mm, the temperature changes were near to the bulk liquid temperature of 80°C, as it can be seen in the first plot of Figure 2.12. The second plot obtained for 3.253 mm height shows

rectangular-shaped temperature signals. The upper-flat temperature of the signal represented the reach of the saturation temperature (T_{sat}), meaning that the measurement has been made in the interior of the vapour mass. However, rapid temperature drops also can be seen due to the release of the vapour mass and consecutive contact with the liquid. At this distance the formation and periodic detachment of vapour masses occurs. Next, 0.353 mm away from the heating surface, the time it took for the signals to indicate the saturation temperature is prolonged as seen in the third diagram. Also, the temperature gradients are much more severe. The explanation for this is the continuous detachment of the vapour masses. Consecutively measuring at 0.123 mm away from the surface, the microthermocouple was partially in a superheated liquid layer. When MTC was placed even lower, it clearly showed the presence and temperature fluctuation inside the superheated thermal boundary.

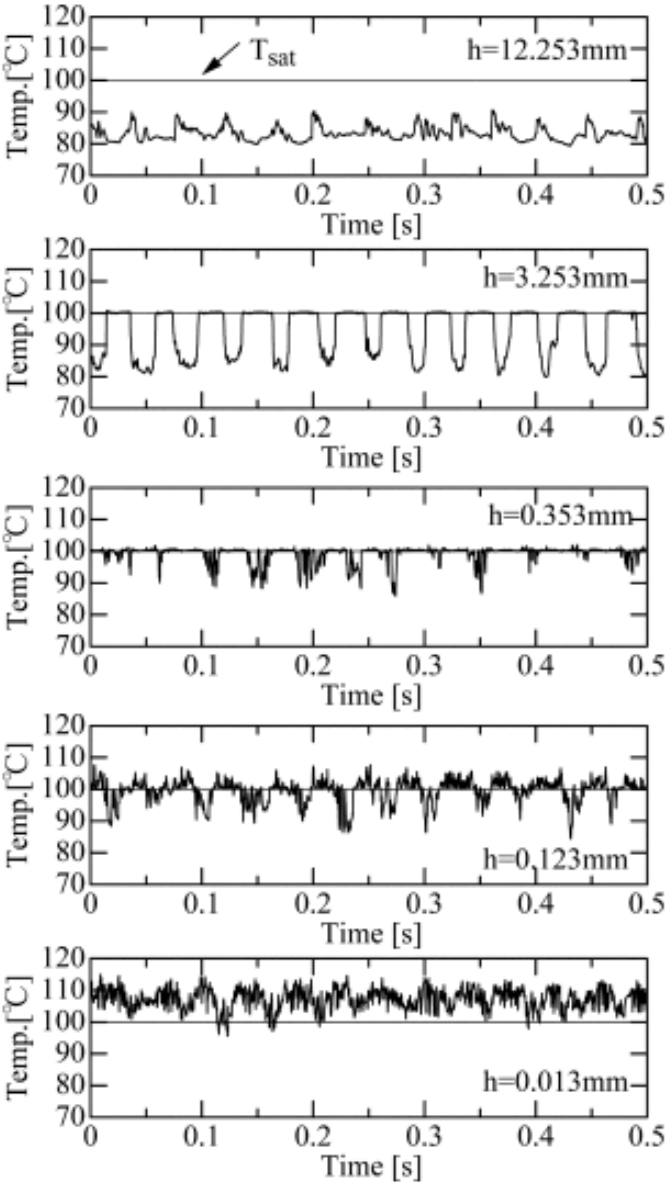

Figure 2.12: Measured temperatures at different heights from the heating surface and 2.67 MW/m^2 and 20 K subcooling. [14]

In conclusion, this study gave an experimental prove about the dynamics of the vapor formation and bubble detachment, as well as the information about the thickness of the thermal boundary layer (TBL) as the microthermocouple approached the surface.

2.2.3 Review of other methods for in-liquid temperature measurement during boiling

In addition to thermocouple measurements, there have been several other attempts to measure in-liquid temperatures during boiling, namely the entire temperature fields and not only the single-spot values. The outlook of results from other authors is shown in Figure 2.13. Despite the advanced approaches and novel equipment, all of these methods have at least one critical drawback that still prevents gaining a breakthrough results. Phase-shift interferometry [15], for example, is characterized by a data reduction process that becomes error-prone for relatively weak thermal gradients. Measurements based on the schlieren effect [16] are strongly affected by the resolution of the rainbow filter and require the use of an expensive high-speed, high-resolution color camera. Two-color laser-induced fluorescence [17] is limited by the susceptibility of the dyes to photobleaching, the temperature sensitivity of the emission peaks, and the attenuation of the excitation light on its path. That said, the microthermocouple approach is still interesting and very much advanced method, even though it only provides a single-spot measurement, but is on the other hand accurate, responsive and straightforward invasive approach.

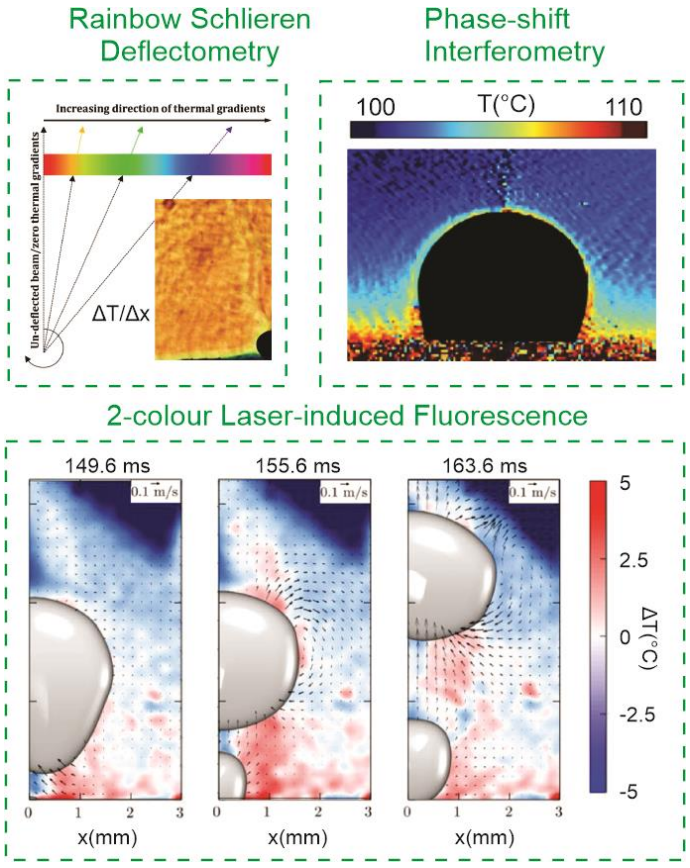

Figure 2.13: Current state-of-the-art of the techniques to measure the temperature around the bubbles during boiling process. [15]–[17].

3 Research methodology

In order to obtain data for the subsequent analysis of the results, we performed three different tests and utilized three different experimental setups. Namely, the static test, the dynamic test and the boiling test. All these experiments, although they differ in the situations in which the results are obtained, utilize the same thermal chamber and data acquisition device. This is described hereafter.

3.1 Data acquisition system

One of the most important requirements to measure the temperature via thermocouple is a high-resolution data acquisition system. Secondly, as we used the direct voltage measurement without internal thermistor in the data acquisition, we used a thermal calibration bath. Keeping that in mind, we were able to perform the temperature measurement in a unknown process (i.e., boiling), as well as known process (i.e. hot thermal bath) during calibration procedure (see Figure 3.1). To process the data and convert voltage measurement to the temperature, a Dewesoft, X software was used.

For analogue to digital conversion (ADC) we used MonoDAQ E-STG device, which has a 24-bit sigma-delta converter and is able to acquire measurements with 20 kHz. This 24-bit resolution was used in a voltage range of 0–100 mV, which provided a theoretical voltage resolution of 6 nV. Considering the Seebeck coefficient of 40 μV/°C, this means we are theoretically able to detect a temperature change of less than 0,001 °C. In reality, we are limited by the noise and the actual resolution is around 10-times of the theoretical value.The wiring diagram of the thermocouple to the ADC is shown on Figure 3.2 and the entire measurement chain is shown on Figure 3.3.

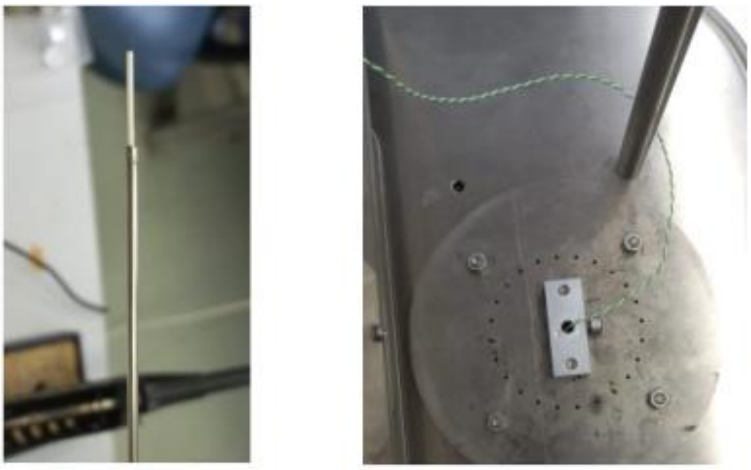

a) *b)*

Figure 3.1: (a) Used microthermocouple and (b) a thermocouple placed inside the hot calibration bath.

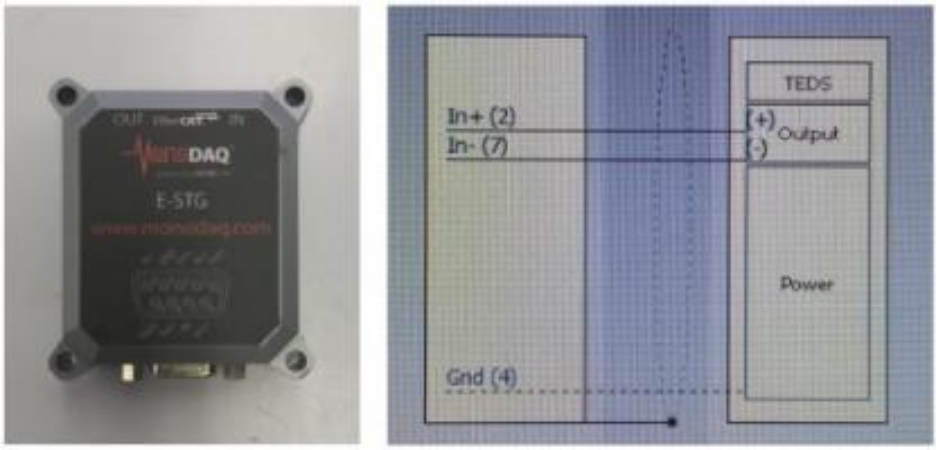

a) *b)*

c)

Figure 3.2: (a) MonoDAQ E-STG card, b) schematics of the thermocouple input and (c) actual wiring at the DSUB 9-pin connector.

The data sent from the data acquisition device was processed and stored in the computer. In addition, thanks to the Dewsoft X software, we can view the data at the same time as it is measured and perform the transformation from voltage difference to temperature. This data was continuously stored in the computer's hard drive.

With the setup shown on Figure 3.3 we carried out two different experiments to characterize the microthermocouple and compare its behavior against classical K-type thermocouple made of thicker wire. Static and dynamic tests were executed, as explained hereinafter.

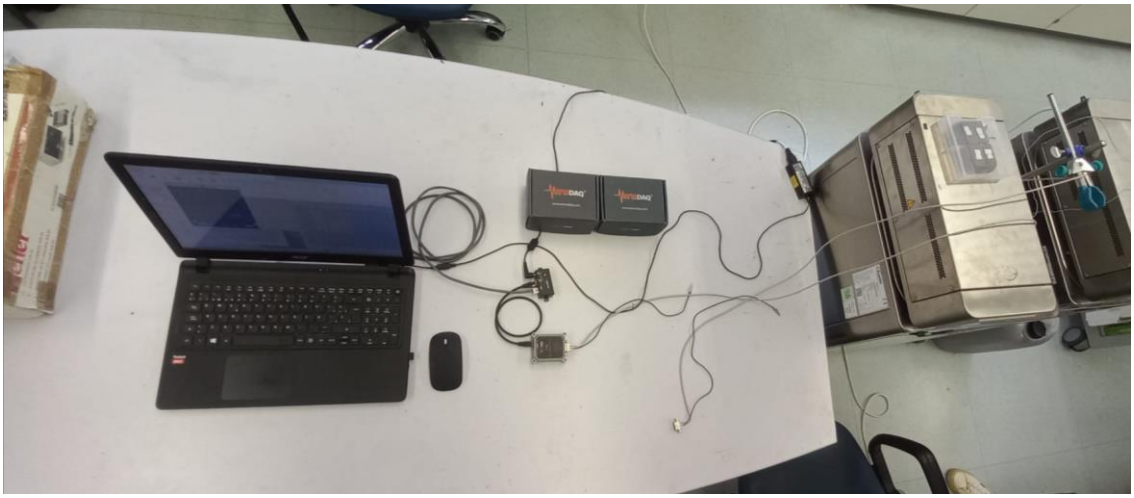

Figure 3.3: Data acquisition system setup used in the laboratory.

3.1.1 Static test with thermocouple and microthermocouple

During this experiment we measured the temperature in two calibration baths, cold and hot, which characteristics are shown in Table 3.1.

Table 3.1: Specifications of the calibration thermal baths.

Property	Value (hot bath)	Value (cold bath)	Unit
Type	Kambič OB-7/2	Kambič OB-7/2 LT	/
Temperature range	40 – 250	-40 – 130	°C
Electrical power	2100	2500	W
Temperature stability	< ± 0.005	< ± 0.005	°C
Temperature uniformity	< ± 0.007	< ± 0.007	°C
Temperature control	PID	PID	/

The thermocouple and micro-thermocouple were introduced in the hot calibration bath where we set up the temperatures gradually from 80°C to 140°C, while the reference junction of the thermocouple was place in a cold bath at a constant temperature of 0 °C (Figure 3.4). As mentioned in the previous chapter, our ADC device did not include internal thermistor and so the reference bath is always needed for absolute temperature measurements.

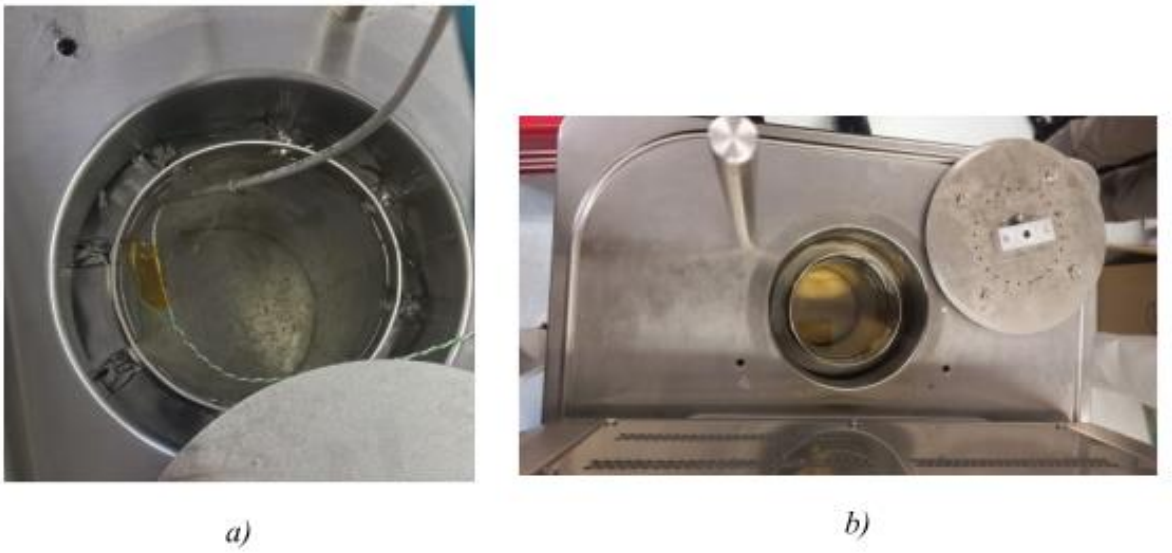

Figure 3.4: (a) Reference junction placed in a cold bath and (b) thermocouple placed in a hot bath.

First, the calibration baths were set to the desired temperatures and kept for 30 minutes to stabilize. While the cold bath was set to 0ºC in all measurement procedures, in the hot calibration bath we varied the temperature from 80ºC to 140ºC progressively, with a difference of 5ºC between calibration steps. The entire measurement chain is shown on Figure 3.5.

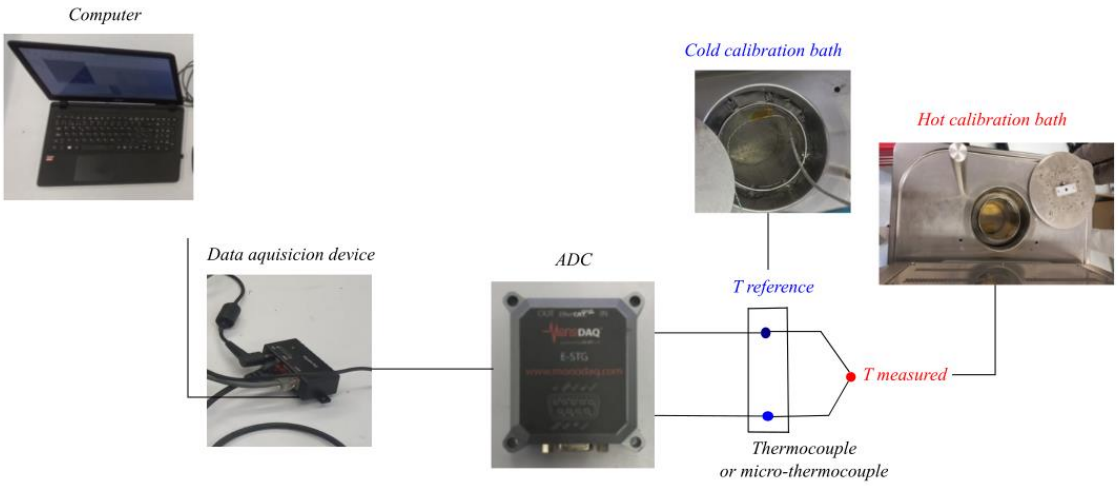

Figure 3.5: Experimental setup for static calibration tests.

3.1.2 Dynamic test with thermocouple and microthermocouple

The goal of dynamic test was to measure the transient response and compare a thermocouple to the microthermocouple. It is expected that microthermocouples provide faster responsiveness to sudden changes whin temperatures. In our case, we dropped a droplet of water to a (micro)thermocouple tip to simulate an input step function, while the readings were measured with ADC with 10 kHz. The warm water droplet was put into a syringe to be able to notice a decent temperature increase above the ambient temperature during each

repetition of the test. The process was repeated several times and the results were later processed as it will be shown in the next chapter of the thesis. In order to confirm that droplet covered the entire (micro)thermocouple tip, a high speed camera (Photon FASTCAM MINI UX100) with dedicated macro lens was also used (i.e. see .Figure 3.6)

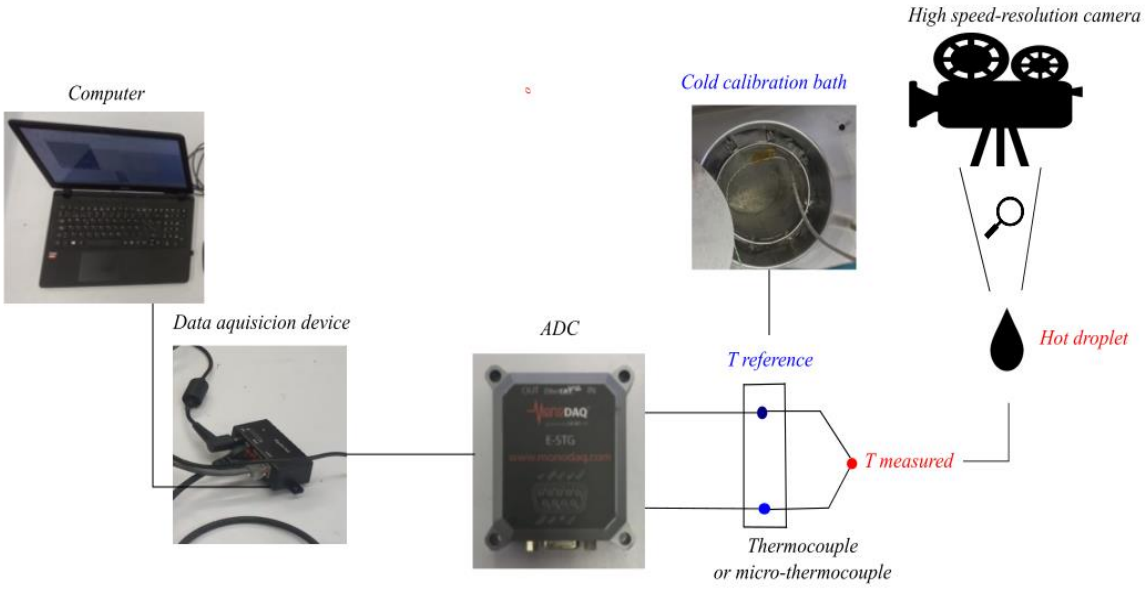

Figure 3.6: Experimental setup for dynamic resposnse tests.

3.1.3 Boiling test with thermocouple and microthermocouple

In order to observe the difference in measurement of the microthermocouple and the thermocouple in a boiling situation, two different types of experiments were performed. The first experiment was dedicated to the detection of the thermal boundary layer (TBL) in single-phase heat transfer conditions, while the second experiment is the analysis of the life cycle of a bubble during boiling.

3.1.3.1 Detection of thermal boundary layer with thermocouple and microthermocouple

The aim of this experiment is to detect the position of the thermal boundary layer from the heated surface. This was performed by measuring the temperature with the thermocouple and the microthermocouple at different distances from the heated surface. It should be added that with the help of the high-resolution camera and high-magnification long distance microscope, these distances could have been determined relatively accurately. In addition, an infrared camera was used in the experiment to determine surface temperature and the heat flux in order to comprehensively confirm the results.

Essentially, our boiling investigation used similar experimental apparatus as detailly explained in a recent study [18]. Here we provide only the important additional information related to repeatable creation of thermal boundary layer and positioning of the (micro)thermocouple. The procedure was the following: A certain current and voltage was set with a variable transformer to preheat the fluid inside the boiling chamber, which was filled with distilled water, until we reached a determined temperature called T_{bulk}. When the

T_{bulk} was reached, the transformer was set to zero, stopping the preheating, and DC current supply was turned on to perform Joule-heating of the boiling surface (25-µm thick stainless steel foil, shown on Figure 3.7). This power supply resulted in a certain heat flux that heated up the foil and created a convective heat transfer between the foil and bulk liquid. Over time, the thermal boundary layer was created. Two tests were carried out, each with different heat fluxes. The first had a heat flux of 5 kW/m^2, while the second had a heat flux of 7.5 kW/m^2.

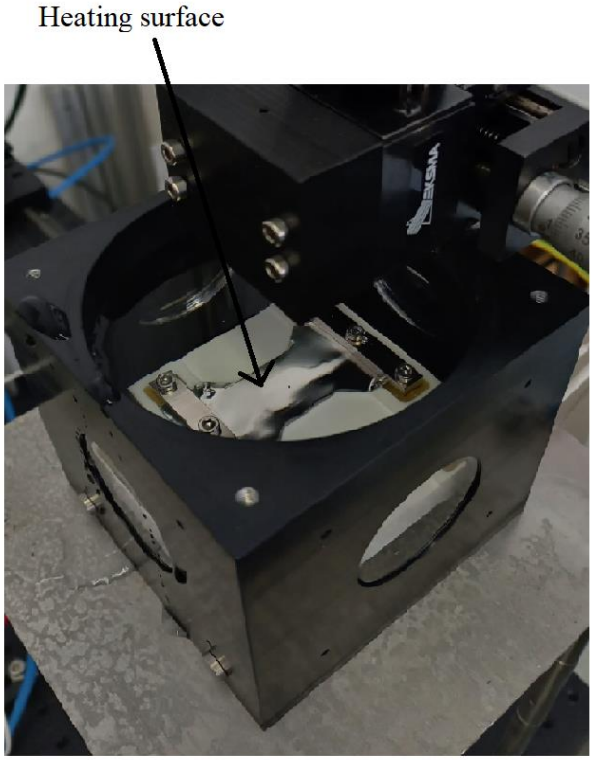

Figure 3.7: Experimental boiling chamber.

Subsequently, different measurements with the thermocouple and the microthermocouple were carried out. These measurements were stored with the help of the Dewesoft X software. Once the various temperatures had been measured and the heat flux of the heated surface had been stored in the infrared camera, the distance of the measuring device from the heated surface was varied, bringing it closer to the surface with each experimental run. In total, we performed seven temperature measurement runs for seven different heights for each of the 5 kW/m^2 and 7.5 kW/m^2. The entire experimental setup is show on Figure 3.8.

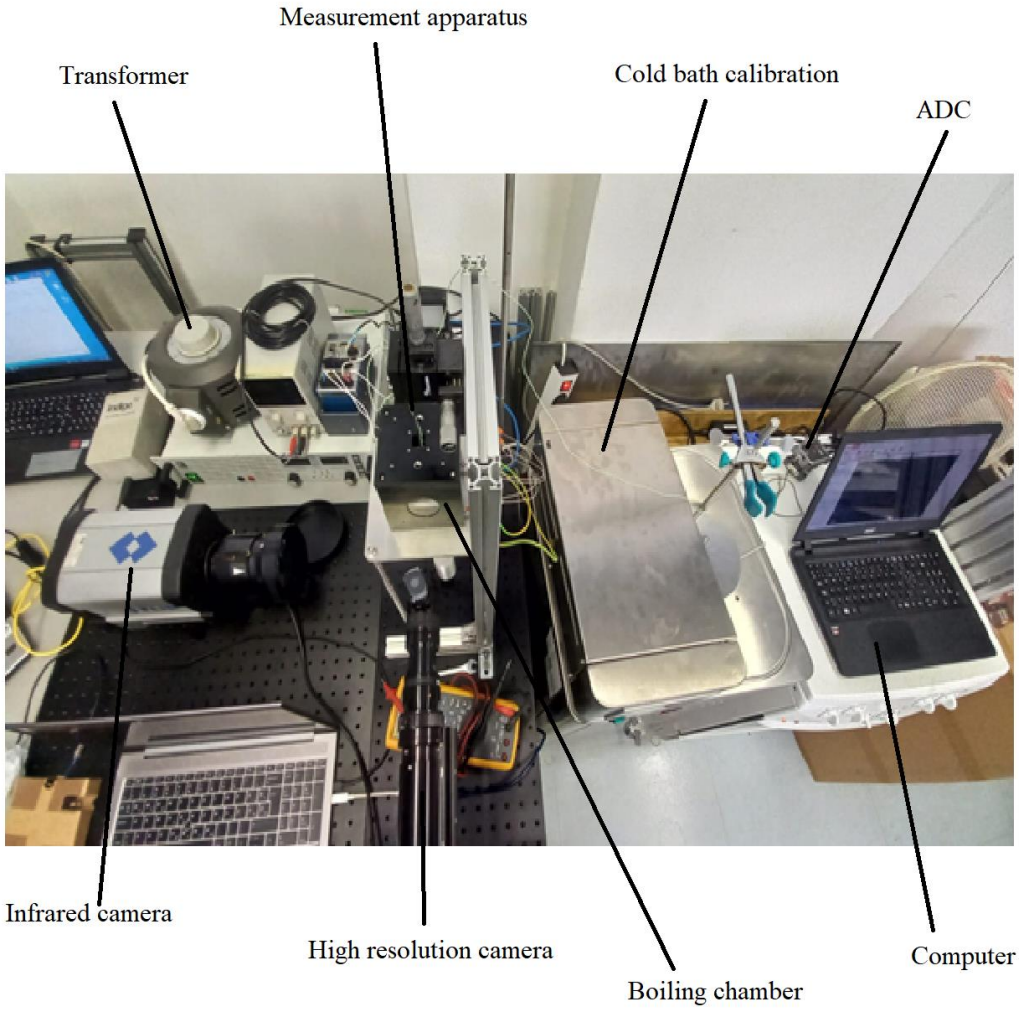

Figure 3.8: Pool boiling experimental setup.

3.1.3.2 Bubble life cycle test with thermocouple and micro-thermocouple

This experiment utilized the same experimental setup as for TBL measurements. The temperature measurement procedure was carried out at different heights above the heated surface, the data was stored and later post-processed. In addition to the previous experimental runs, this time we aimed to also measure the temperature fluctuations around the formation of a bubble at a nucleation point. This experiment is intended to confirm the behavior of the fluid around the bubble life cycle at the nucleation point, as discussed in the chapter explaining the theoretical background.

This time the heat flux was set above 7.5 kW/m^2 and the nucleation was triggered at an artificial nucleation site (Figure 3.9) in the center of the foil. This site was created via laser texturing [19], followed by a drop casting of hydrophobic FDPA chemical to render the surface superhydrophobic. With this procedure, we were able to create stable nucleation site and to keep the distance of the microthermocouple constant relative to the point of bubble nucleation. After switching off the cartridge heaters and setting on the DC power supply through the foil, the formation of a bubble took place followed by its growth and detachment. After finishing this procedure for a certain microthermocouple height, we changed the

distance by bringing the measuring device closer to the heated surface and performing the same measurement again. This procedure was performed six times in total, five times around the nucleation point and once inside the bubble.

During this experiments, the IR camera was also used in order to determine the position, transient temperature and local heat flux field at the boiling surface. On the other hand, the synchronized high-resolution camera was also used to record hbubble dynamics and to confirm thermocouple position.

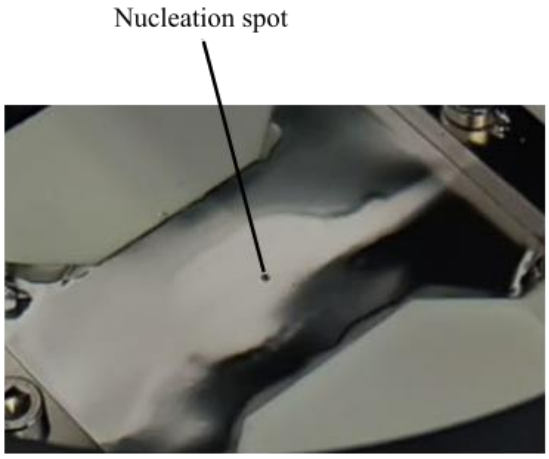

Figure 3.9: Artificial nulceation site on the thin metal foil.

4 Results and discussion

This section shows the results of static and dynamic calibration tests as well as boiling experiments together with discussion supporting the findings.

4.1 Static tests and calibration curves

After obtaining the results with the thermocouple and the microthermocouple, the data was plotted and compared for both thermocouples.

4.1.1 Test with classical K-type thermocouple

As can be seen in the table Table 4.1 the difference between the exact temperature of the process and that measured by the thermocouple is relatively small, up to 2,1%.

Table 4.1: Experimental thermocouple data in static calibration test.

$T_{process}$ ºC	T_{ref} (ºC)	ΔV (U)	$T_{measured}$
85	0	0,003459	86,49
90	0	0,003666	91,65
95	0	0,003872	96,85
100	0	0,004077	101,92
105	0	0,00429	107,17
110	0	0,0045	112,36
115	0	0,004707	117,67
120	0	0,004913	122,82
125	0	0,005117	127,91
130	0	0,005321	132,97
135	0	0,005523	138,11
140	0	0,005726	143,11

From the measured voltage, we first calculated the temperature based on theoretical Seebeck coefficient of 40 μV/°C. However, as can be seen in the Figure 4.1, the coefficient of the thermocouple used in the test was not exactly 40 μV/°C, because the line given by the measurement overestimates the actual process temperature set inside the hot calibration bath. Calculating a Seebeck coefficient for each voltage value, using the actual temperature of the process, and averaging the obtained results, the actual Seebeck coefficient of the experiment's thermocouple is determined to be 40.855963 μV/°C. Figure 4.2 displays the fitted line with the calculated coefficient, which is later used as the actual value. It is important to note that this procedure should be undertaken for each new (micro)thermocouple. The reason is that thermocouples are never the same among each other mainly due to the stochastic nature ow the weld at the thermocouple tip.

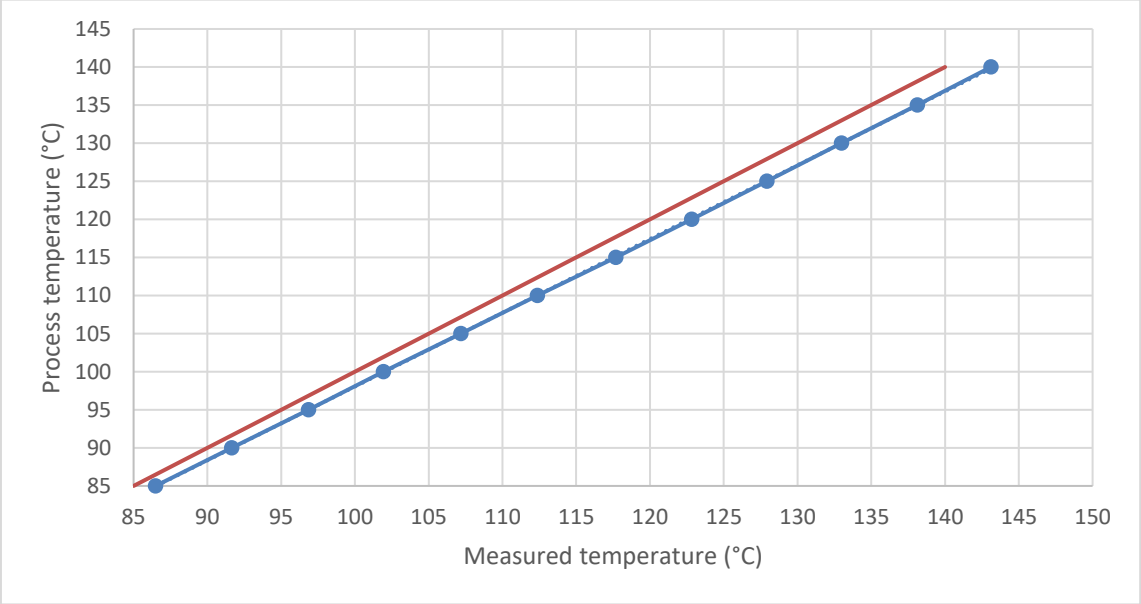

Figure 4.1: Comparison between measured and actual temperatures for static test with thermocouple – theoretical Seebeck coefficient.

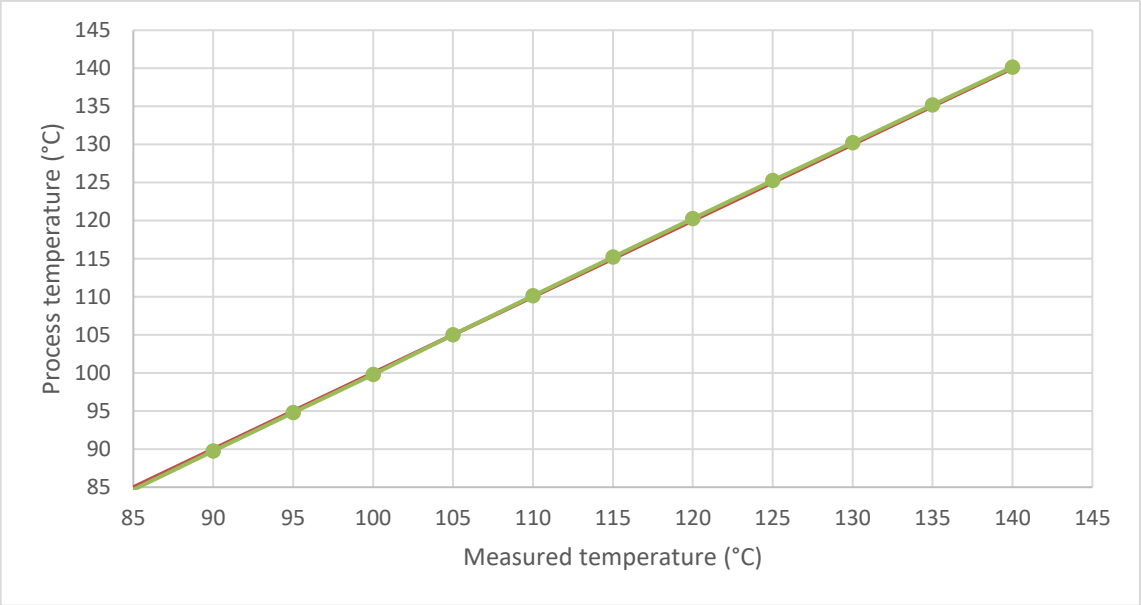

Figure 4.2: Comparison between measured and actual temperatures for static test with thermocouple – experimentally determined Seebeck coefficient.

4.1.2 Test with K-type microthermocouple

Repeating the same procedure as with the thermocouple, the same methodology is applied to determine the Seebeck coefficient for microthermocouple. The experimental data obtained is shown in Table 4.2:

Table 4.2: Experimental microthermocouple data in static calibration test.

$T_{process}$ ºC	T_{ref} (ºC)	ΔV (U)	$T_{measured}$
85	0	0,003429	85,76
90	0	0,003637	90,93
95	0	0,003845	96,11
100	0	0,00406	101,48
105	0	0,004266	106,66
110	0	0,004476	111,9
115	0	0,004684	117,09
120	0	0,004892	122,3
125	0	0,005094	127,35
130	0	0,005301	132,53
135	0	0,005504	137,58
140	0	0,005708	142,64

Based on the results in Figure 4.3, we computed the new experimentally determined Seebeck coefficient for microthermocouple and found to be 40.6428 μV/°C as presented in Figure 4.4.

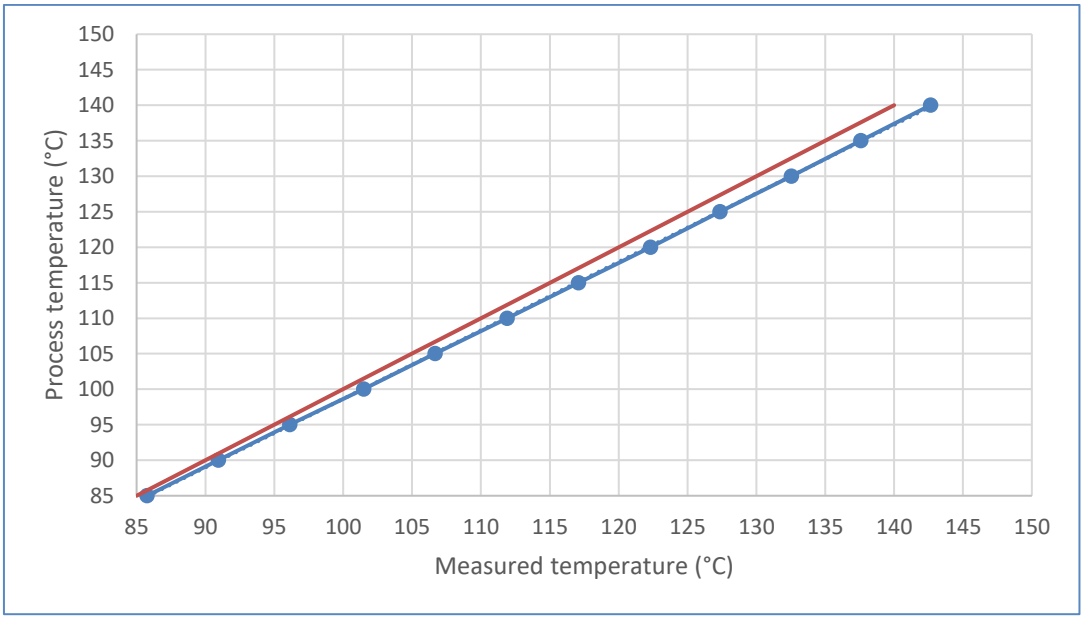

Figure 4.3: Comparison between measured and actual temperatures for static test with microthermocouple – theoretical Seebeck coefficient.

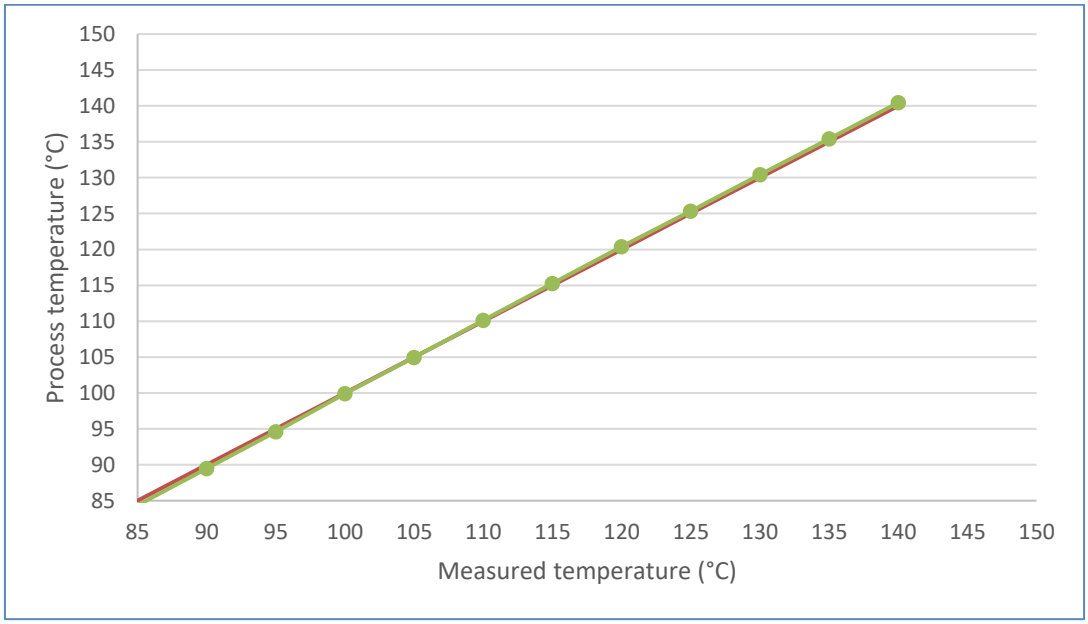

Figure 4.4: Comparison between measured and actual temperatures for static test with microthermocouple – experimentally determined Seebeck coefficient.

4.2 Dynamic tests

To partially characterize the response time of the thermocouple and microthermocouple, we conducted dynamics test with a heated droplet and measure the high-speed data as explained in previous chapter of the thesis. Results obtained at 20 kHz were filtered using the moving-average approach and then compared. In addition, a high-speed camera simultaneously captured the contact of droplet and thermocouple, example of which is also shown hereinafter.

4.2.1 Dynamics test with regular K-type thermocouple

After dropping a warm droplet on a thermocouple, a drastic change in the signal was detected at the instant of 14.2494 seconds. In order to calculate the reaction time for the temperature variation of the thermocouple, we first filtered the signal using a moving average approach. Results are shown on Figure 4.5. Afterwards, the values were normalized to become unitless and are shown on Figure 4.6. Time constant was determined as the time when a signal response reaches 63,2 % of the input step function value. Comparison between thermocouple and microthermocouple is shown later.

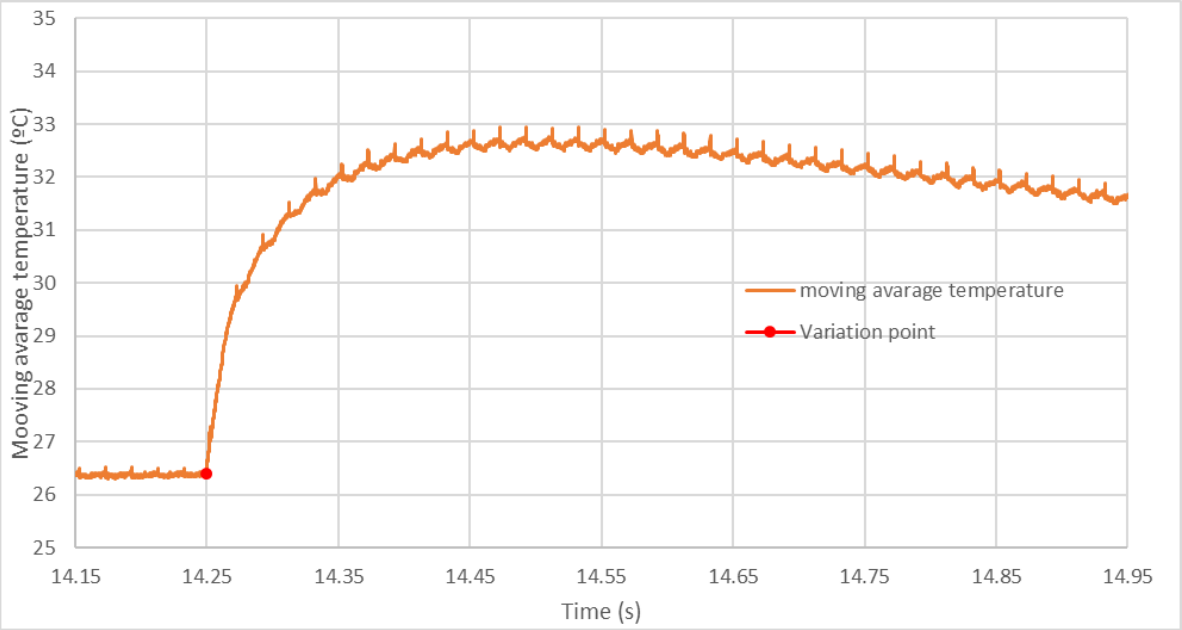

Figure 4.5: Temperature variation measured with thermocouple with filtered noise.

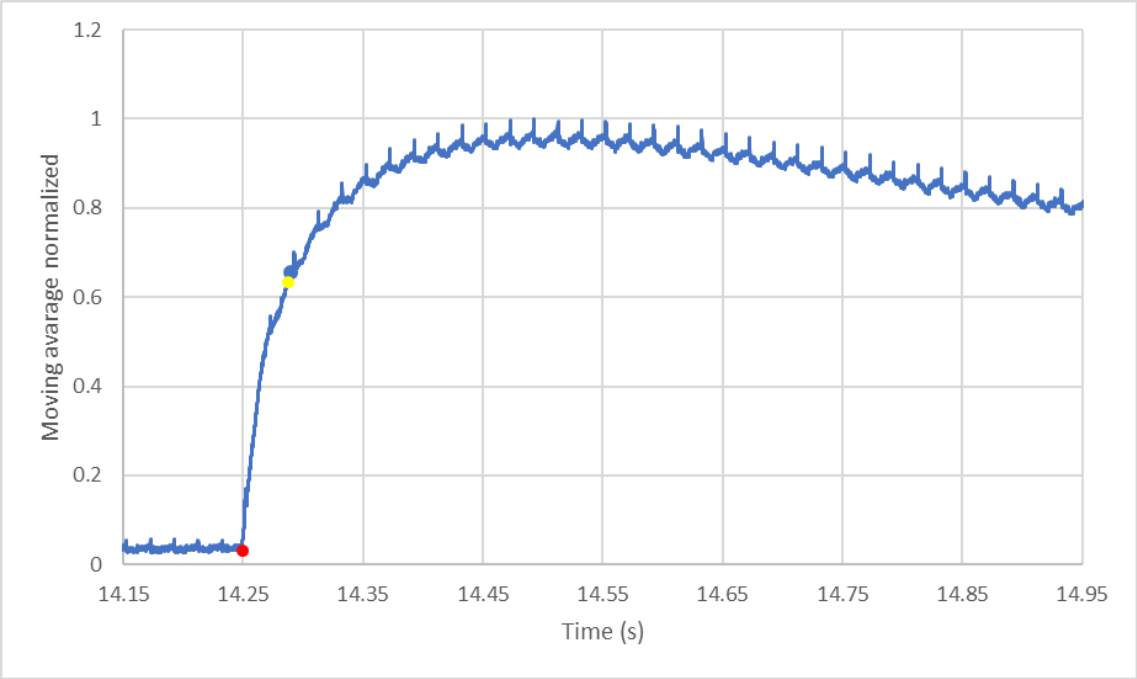

Figure 4.6: Normalized temperature variation measured with thermocouple with filtered noise.

Figure 4.7 shows three instances how droplet contacts the thermocouple and covers it completely. Water in particular has a good thermal transport properties and provides high effective heat transfer coefficient on the wall of the thermocouple tip (probably more than 300 W/m^2K), which is good to determine thermal response for water-based application such is nucleate boiling. In air or some other liquid, the response of the thermocouple could be much slower. That said, the response time of this particular device depends on the conditions it is being used in.

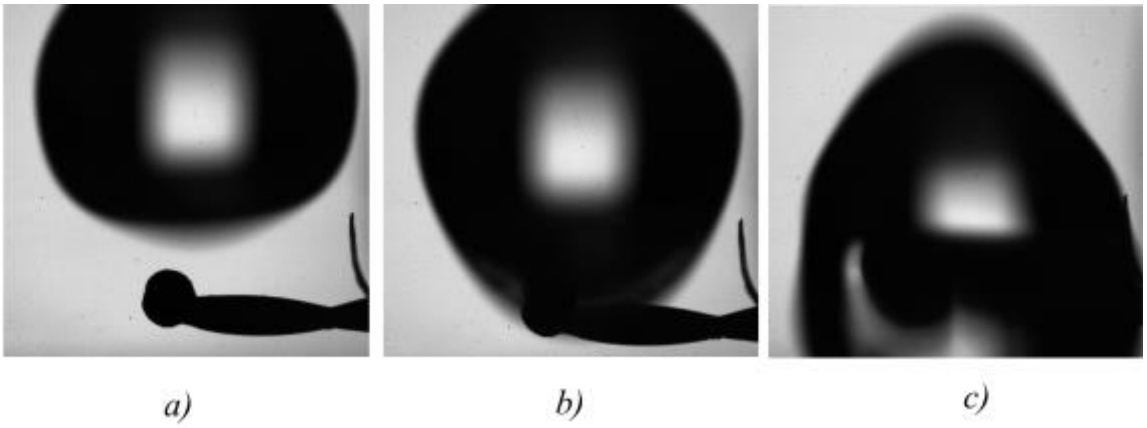

Figure 4.7: a) Warm droplet (a) before, (b) during and (c) after contacting the thermocouple.

4.2.2 Dynamic tests with K-type microthermocouple

Positioning the microthermocouple very carefully so that it would not break, we performed the same experiments as explained in previous chapter. In this case the microthermocouple detected a much more drastic increase (gradient) in voltage and temperature. This is because the microthermocouple is much smaller in mass, which responds significantly faster to any changes in the surroundings. In experiment with the microthermocouple, we can find the variation point at 1.8896 seconds. The same as with previous data, filtering was applied also here and the temperatures were then normalized, as shown on Figure 4.8 and Figure 4.9.

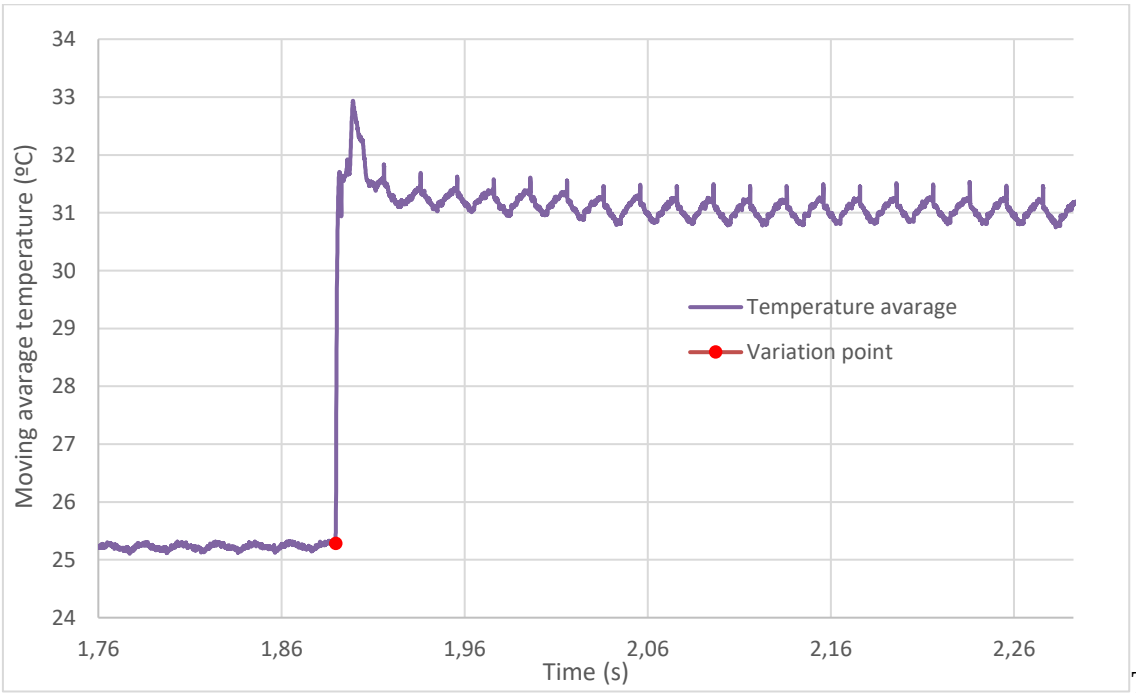

T

Figure 4.8: Temperature variation signal without nose of the microthermocouple.

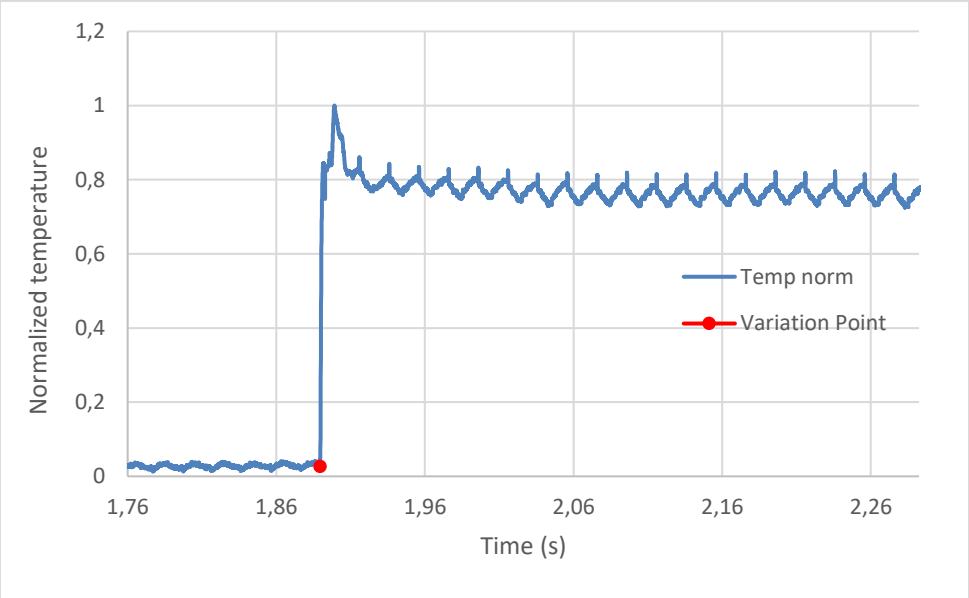

Figure 4.9: Normalized moving average temperature in order to calculate the reaction time of the microthermocouple.

It is worth noting that the micro-thermocouple is a much more sensitive but more precise measurement tool, which is also seen on the high speed images in Figure 4.10. With this observations, we can make a number of assumptions about the dynamic behavior of the microthermocouple explained in the comparison section. Based on the actual measured dimension of the microthermocouple tip and assumed thermal properties, one could also determine theoretical thermal response time based on lumped-capacitance model and assumed effective heat transfer coefficient.

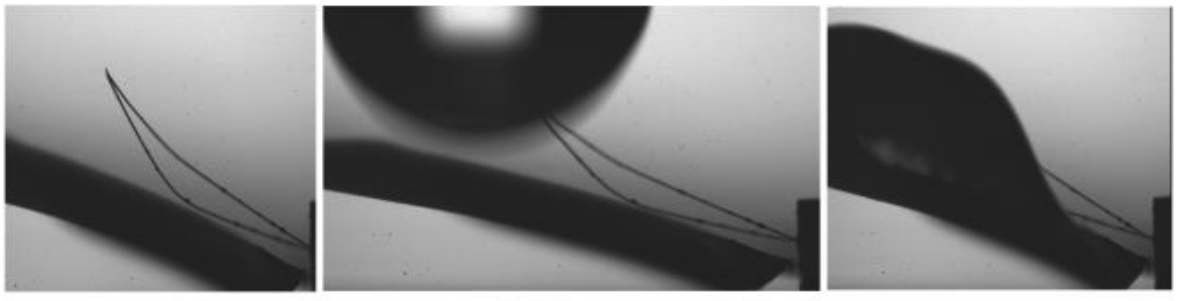

Figure 4.10: a) Warm droplet (a) before, (b) during and (c) after contacting the microthermocouple.

4.2.3 Comparison between thermocouple and microthermocouple

As we have seen on previous Figures, the microthermocouple reacts much faster to the thermal disturbance than the normal thermocouple. This difference in the reaction time can be determined by the thermal time constant (τ). This value corresponds to the difference in

time between the variation point and the point corresponding to the value of $1-(e^{-1}) = 0.632$ from the normalized moving average temperature, as shown in Figure 4.11.

In Figure 4.11 we can see the values for τ and their corresponding times for both the microthermocouple and the thermocouple. The Table 4.3 also shows how the microthermocouple is 0.0377 seconds faster than the thermocouple, which means that the microthermocouple being 48.125 times faster than the thermocouple, an abrupt difference when measuring precision is required.

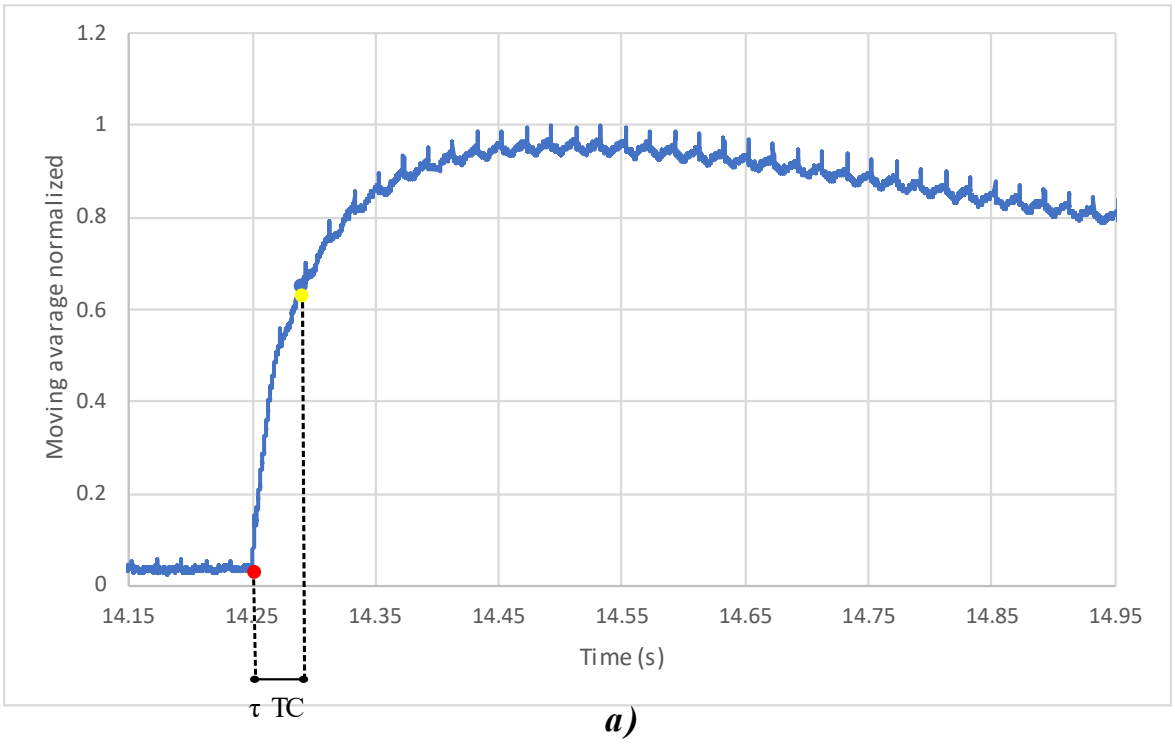

a)

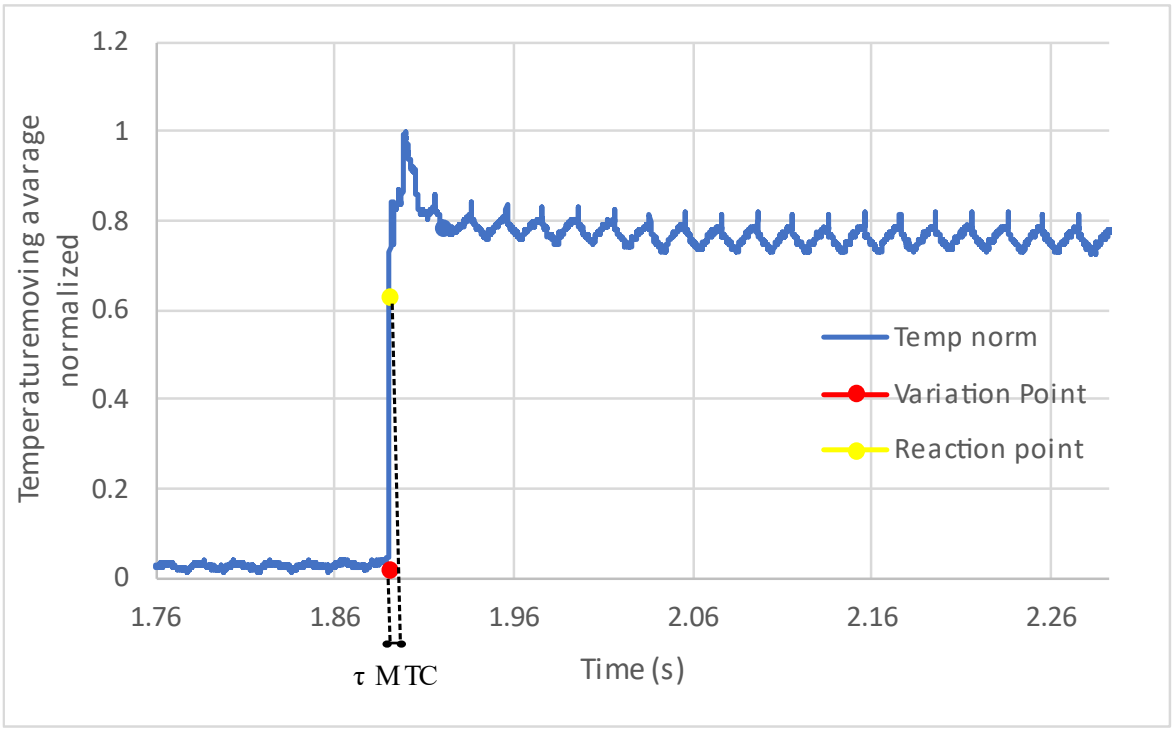

b)

Figure 4.11: Thermal time constant representation for (a) themocouple. (b) microthermocouple.

Table 4.3: Determination of τ value for the thermocouple and microthermocouple.

	a)Variation time (s)	**b)Time at 1-(e^{-1}) from the normalised moving average temperature. (s)**	**τ = b – a (s)**
Thermocouple	14.2494	14.2878	0.0385
Microthermocouple	1.8896	1.8904	0.0008

If the experiment had been performed by measuring simultaneously with both the thermocouple and the microthermocouple, and see the measurements variation at the same time instant, it would have been the micro thermocouple that would have captured the temperature difference faster and more accurately, as can be seen in Figure 4.12. This leads to the conclusion that the microthermocouple, not only is a more accurate measurement tool than the thermocouple, but also gives a faster response to a dynamic situation.

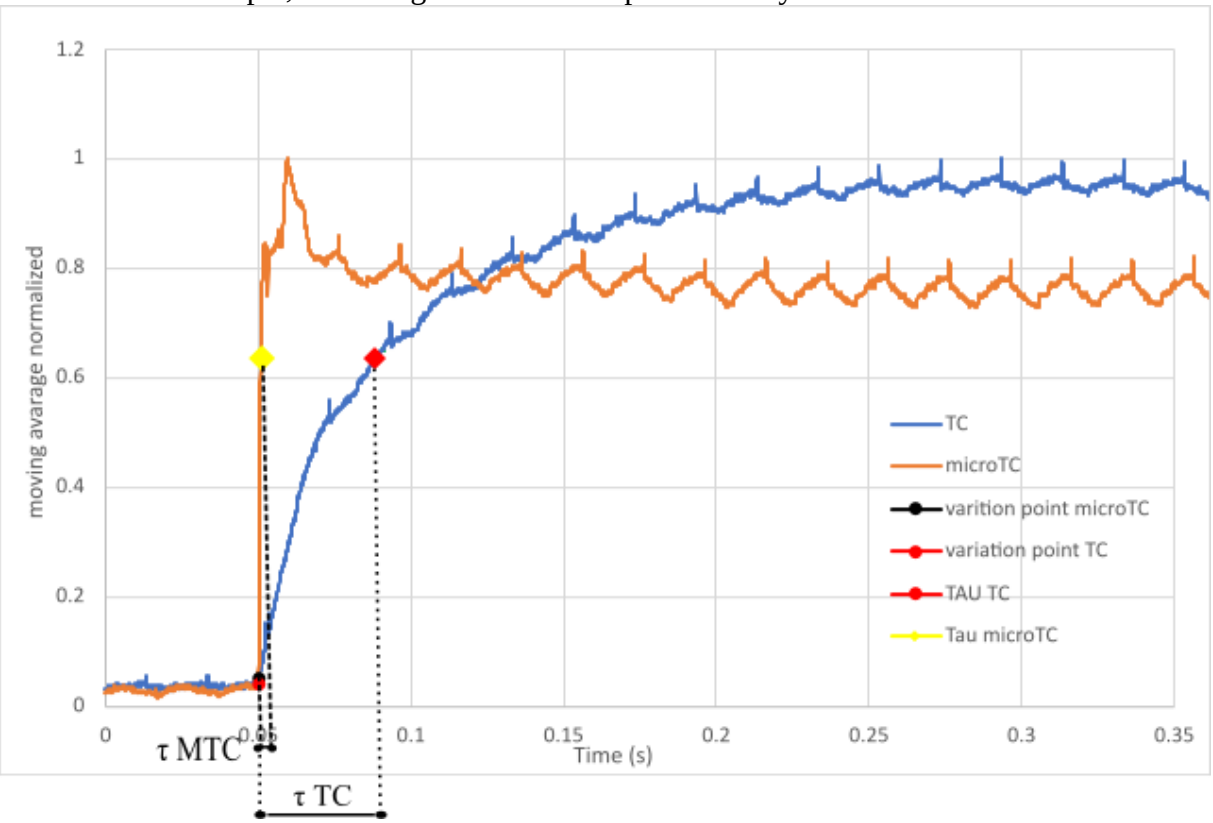

Figure 4.12: Difference between τ value for the thermocouple and microthermocouple when the variation is produced at the same time.

4.3 Results obtained within the thermal boundary layer

Thanks to the set-up described in the section on the data acquisition system for the boiling tests, we have obtained a series of results for both the thermal boundary layer experiment and the bubble life cycle analysis. These results will be discussed in the following sections. It is recalled that all these results confirm the difference in the behavior of the microthermocouple compared to the thermocouple when measuring certain parameters, in particular temperature, in a boiling environment.

4.3.1 Thermal boundary layer analysis with regular K-type themomocouple

In this experiment we have obtained a series of results which allow us to determine the position of the thermal boundary layer. As mentioned above, by applying a certain current and voltage, i.e. a determined power to a certain area, we have been able to establish an specific heat flux. By measuring the temperature over time at different distances from the heated surface, we have obtained a series of results for both the thermocouple and the micro thermocouple.

In the case of the thermocouple, two tests were carried out by applying two different currents (I) and voltages (ΔU) to produce the heating of the surface where all the parameters were measured. With these results and knowing that the effective heated area (A) is 0.0018 m^2, given the equation for the heat flow dissipated by the Joule effect ($\dot{q}$), we can determine approximate heat flux as shown in Table 4.4.

$$\dot{q} = \frac{\Delta U \times I}{A} \tag{4.1}$$

Table 4.4: Voltage, current and heat flow used and the two tests for boundary layer thermocouple experiments.

	Voltage (V)	Current (A)	Heat Flux (kW/m^2)
Test 1	0.85	10	5
Test 2	1.08	12.5	7.5

With the heat fluxes of the different tests, the distilled water inside the boiling chamber was preheated up to 96.5ºC in all the thermal boundary layer experiments. Once this temperature was reached, the foil (surface) was heated, and various temperatures were measured over time for the seven different heights with respect to the heated surface. To find out the value of these heights, we used MATLAB software to measure the coordinates of the thermocouple and the heated surface. The difference between these coordinates was the distance at which we made the measurements, but this distance was given in pixels (Figure 4.13). With a scale factor of 13 micrometres per pixel, we were able to obtain the different physical values of the heights given in the Table 4.5.

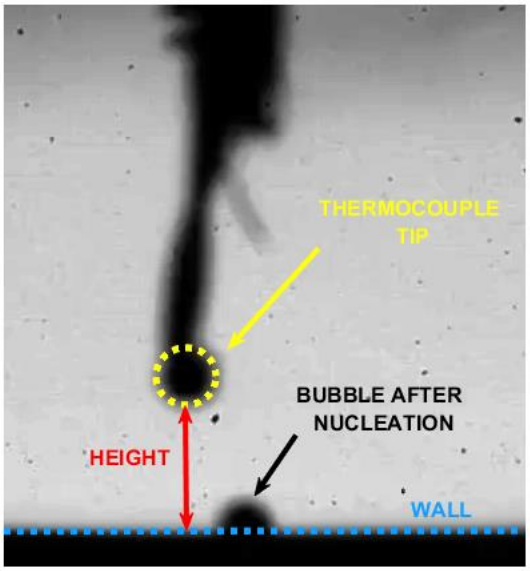

Figure 4.13: Determination of the height of the thermocouple using MATLAB software.

Table 4.5: Results of the heights determinations for the TBL experiment with the thermocouple.

Height	Test 1 (5 kW)	Test 2 (7.5 kW)
h1	4.80 mm	4.85 mm
h2	3.80 mm	4.38 mm
h3	2.80 mm	3.39 mm
h4	1.90 mm	2.49 mm
h5	1.00 mm	1.51 mm
h6	0.15 mm	0.63 mm
h7	~50 µm	~50 µm

It should be noted that the last measurement shows a distance to the heated surface of around 50 µm. This is because accurate determination of the distance above the surface was relatively unacurate. However, the thermal boundary layer, whose position is known to be around 20-100 µm, was detected during the measurements.

After determined height, we carried out the temperature measurements. Once all measurements of temperatures through time were obtained at the different heights with respect to the heated surface, as not all measurements started at the same value of T_{bulk}, they were normalized by subtracting $T(t) - T_{bulk}$. This way, it is possible to visualise how the temperature varies as the thermocouple approaches the heated surface, as can be seen in Figure 4.14 and Figure 4.15.

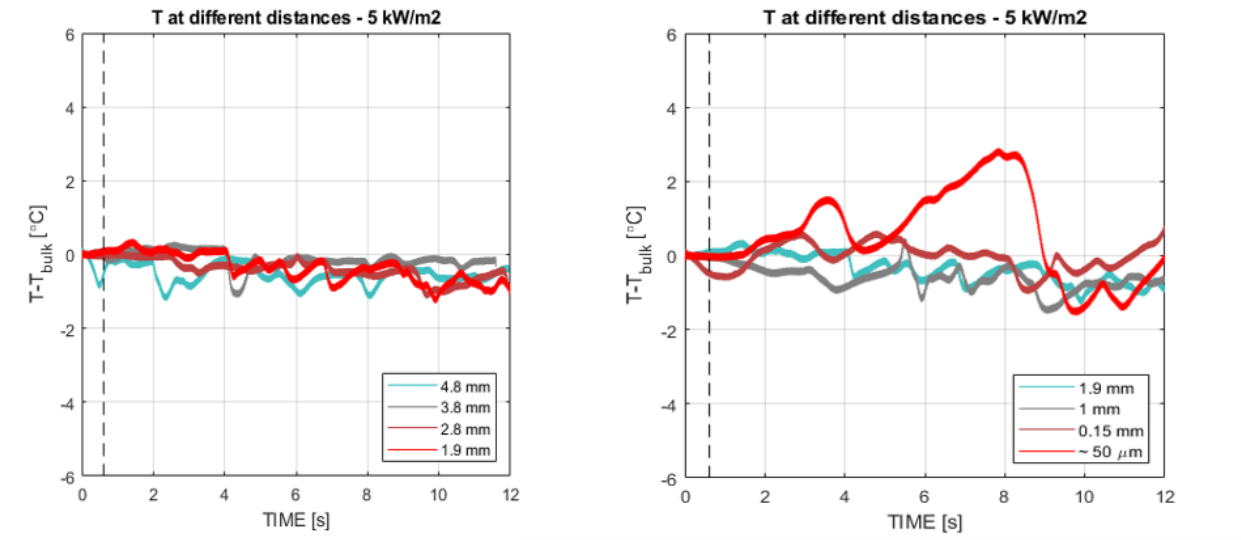

Figure 4.14: Normalized temperature at different heights from the heated surface at the heat flux of 5kW/m^2.

The test with a heat flux of 5 kW/m^2 shows that at distances far away from the heated surface, no large temperature variation is detected. Some slight variations are detected due to small internal fluctuations of the water, but they are not remarkable. However, as the thermocouple approaches the heated surface, these temperature variations increase. This is because the thermocouple gets closer and closer to the thermal boundary layer, where the temperature its higher. It is, in particular, at a distance of about 50 μm where we can observe how the temperature variations are greater, with a temperature difference of up to 2.5ºC with respect to the initial temperature T_{bulk}, i.e. a temperature of 99ºC. It is here that the specific behavior in temperature of the thermal boundary layer can be detected. Also, due to the continuity of mass and the fact that a fluid at a higher temperature tends to have a lower density and rise, these temperature fluctuations are captured more intensely.

Moreover, it is true that the thermal boundary layer in the experiment with 5 kW/m2 is detected, however a better analysis is needed. Therefore, the heat flux was increased to 7.5 kW/m2 (Figure 4.15). Once these parameters were established, the same temperature measurements were made at the different distances from the heated surface (Table 4.5). In these measurements, it can be seen more clearly how the thermocouple, as it approaches the thermal boundary layer, detects a greater temperature variation with respect to T_{bulk}, since the heat flux is greater.

At first, in the 7.5 kW/m^2 test, the same beharviour occurs as in the 5 kW/m^2 test. When heating the surface, no noticeable temperature variation is observed as we are at distances far from the thermal boundary layer [Figure 4.15 (a)]. Particular slight temperature variations can be observed due to the internal fluctuations of the liquid. On the other hand, as we get closer to the heated surface, the temperature variations are considerably larger as seen in Figure 4.15(b). That is because the thermocouple is approaching the thermal boundary layer. It is, in particular, at the same distance of 50 μm from the heated surface that is observed above a 4ºC temperature difference from T_{bulk}, making it a temperature of 100.5ºC in that spot, detecting the thermal boundary layer more clearly than the 5kW/m^2 test. It has to be

noted that for atmospheric boiling of water, the surface superheat and thermal boundary layer must significantly exceed 100 °C to initiate boiling. This measuring principle is therefore good to determine appropriate boundary conditions and to investigate how different wettable surfaces could be used to enhance onset of boiling.

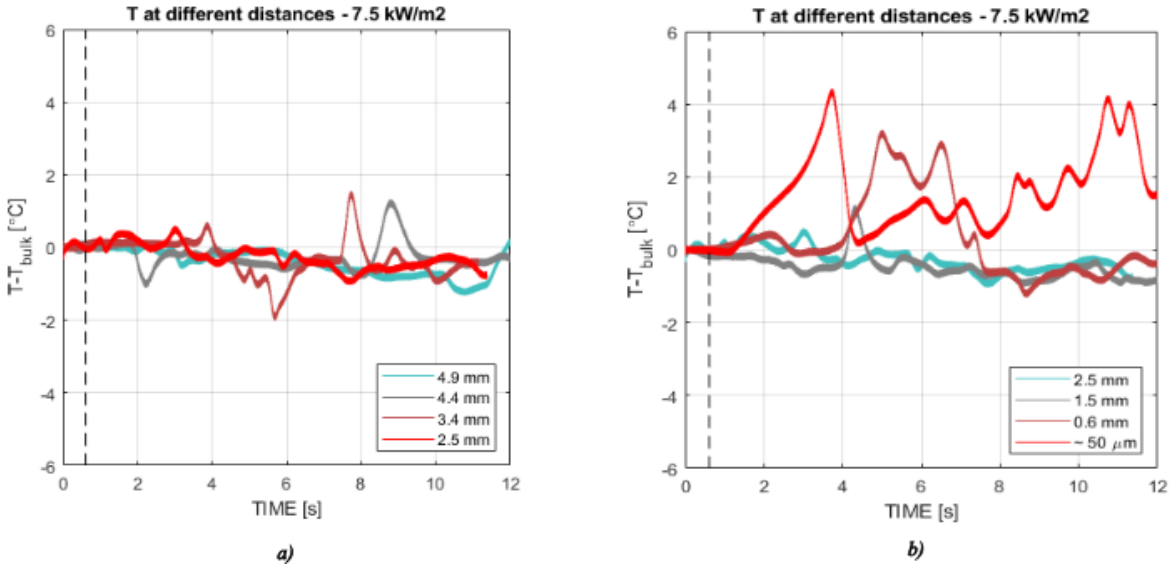

Figure 4.15: Normalized temperature at different heights from the heated surface at the heat flux of 7.5kW/m^2.

4.3.2 Thermal boundary layer analysis with K-type microthermocouple

Thermal boundary layer experiments with the microthermocouple were performed in the same way as with the thermocouple. Two tests were performed with the same heat fluxes as for the thermocouple. The first test had a heat flux of 5 kW/m2 and the second of 7.5 kW/m2. However, different voltages and currents were applied. With these values, knowing the area value and with the Joule effect heat flux equation (4.1), is verified that the heat fluxes, named above, are the same on the heated surface for the thermocouple as for the microthermocouple, as can be seen in Table 4.6.

Table 4.6. Voltage, current and heat flow used ind the two tests for boundary layer microthermocouple experiments.

	Voltage (V)	Current (A)	Heat Flux (kW/m^2)
Test 1	1	9.7	~5
Test 2	1.2	11.5	~7.5

In the case of the microthermocouple, the water was preheated to a temperature very similar but not exactly the same as in the case of the thermocouple. This temperature was around T_{bulk} = 95.5ºC. It must be again emphasized that we must establish the distances of the microthermocouple regard to the heated surface. For the case of the microthermocouple, due to its small size, we used a more accurate scale the in previous study. This scale was now 9 micrometres per pixel (Figure 4.16), while the heights are provided in Table 4.7.

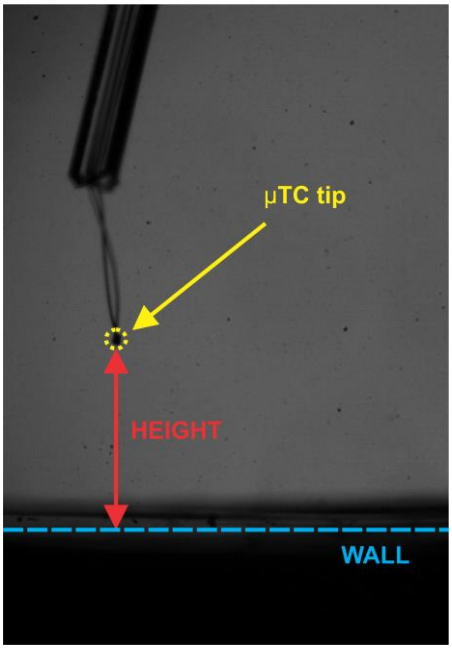

Figure 4.16: Determination of the height of the microthermocouple using MATLAB software.

Table 4.7: Results of the heights determinations for the TBL experiment with the microthermocouple.

Height	Test 1 (5 kW)	Test 2 (7.5 kW)
h1	2.60 mm	2.50 mm
h2	1.80 mm	1.60 mm
h3	0.90 mm	0.70 mm
h4	0.50 mm	0.35 mm
h5	0.25 mm	0.10 mm
h6	0.10 mm	~20 µm
h7	~20 µm	-

It should be noted that the last measurement in each test shows a distance to the heated surface of around 20 µm. This is because the last distance cannot be accurately determined. However, the thermal boundary layer, whose position is known to be around 20-100 µm, was accurately detected during the measurements.

Once the position to be measured is set and the T_{bulk} reaches the desired value, we start storing data and turn on the DC power supply. Once all temperature measurements are obtained over time for all heights, they are normalized as in stury before, by subtracting $T(t)$-T_{bulk}. This is needed to compare how the temperature variation is detected with the microthermocouple as we approach the heated surface for both tests, as it is seen in the Figure 4.17.

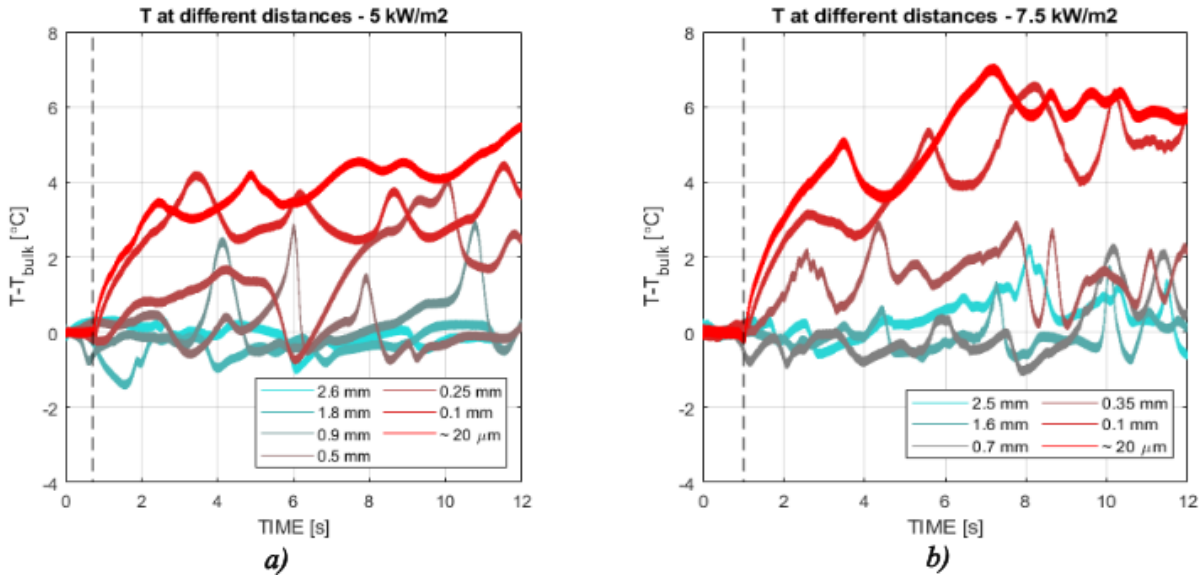

Figure 4.17: Normalized temperature at different heights from the heated surface for a) 5 kW/m^2 and b) 7.5 kW/m^2.

In the case of the microthermocouple, the values are quite different. The measurements were made at initial distances closer to the heated surface. This allowed the position of the thermal boundary layer to be determined more accurately. As can be seen in Figure 4.17, in both tests, at distances further away from the heated surface, there is not a large temperature difference with regard to T_{bulk} over time. There are slight temperature variations due to internal fluctuations in the water. However, as we approach the heated surface, an increase in the temperature difference can be observed. This is due to the fact that we get closer to the thermal boundary layer. Specifically, it is when we are at a distance of 20-100 µm that we detect the thermal boundary layer with temperature difference values up to 5 ºC, i.e. a temperature of 100.5 ºC for the 5 kW/m2 test and 7ºC, i.e. a temperature of 102.5 ºC for the 7.5 kW/m2 test. Thus, the position of the thermal boundary layer is verified experimentally more accurately than with the thermocouple.

Furthermore, if we compare the experiments carried out with the thermocouple and the microthermocouple, it is remarkable how faster the microthermocouple outperforms the thermocouple in detecting the drastic temperature variation. This can be seen by comparing the 50 µm height in Figure 4.14(b) with the 0.10 mm or 20 µm height in Figure 4.17(a) for the 5 kW/m^2 test. The same occurs, and more clearly, if the 50 µm height in Figure 4.15(b) is compared with the 0.10 mm or 20 µm height in Figure 4.17(b) for the 7.5kW/m^2 test.

Moreover, it can be observed that by placing the thermocouple and microthermocouple in the thermal boundary layer, the thermocouple performs the measurements with abrupt changes in the temperature of the thermal boundary layer (50 µm) without reaching a more or less stable temperature, as can be seen in 50 µm of height in Figure 4.14(b) and Figure 4.15(b). The opposite happens with the MTC. When measuring in the TBL height at the 20-100 µm, a certain temperature is reached, which the microthermocouple measures relatively stable compared to the thermocouple for both tests, without sharp decreases as can be observed in the heights 20 µm and 100 µm in Figure 4.17(a-b). This is due to the fact that the tip of the thermocouple is larger than 50 µm (around 1mm), i.e. larger than the position of the thermal boundary layer. Therefore, even if the thermocouple is approached at the

maximum distance from the heated surface when performing the various temperature measurements at the TBL, it also captures the temperatures of the position above the TBL, which are lower in value. Consequently, no uniform and accurate TBL temperatures are measured with the thermocouple, but variable and inaccurate ones. The reverse is true for the MTC. Because the tip of the microthermocouple is around 30 μm or even smaller, it is able to fully penetrate the TBL, allowing accurate and uniform temperature measurements at this position.

In conclusion, it has been observed in this experimental analysis that the microthermocouple reaches the TBL more accurately. This means that it not only detects the temperature of the TBL more accurately, i.e. with minor temperature variations that produce uncertainty, but also detects it more quickly compared to the ordinary thermocouple. In addition, we have also been able to confirm experimentally the position of the thermal boundary layer of a heated surface with two different thermal fluxes, being located for both tests (5 kW/m^2 and 7.5 kW/m^2) in a similar position of between 20-100 micrometres, confirming the theoretical foundations and literature.

4.4 Results and discussions of boiling tests

This experiment consists of the same procedure as the thermal boundary layer experiment. Temperatures are measured over time with the thermocouple and the microthermocouple, bringing them closer and closer to the heated surface. However, in this experiment, a bubble is formed in order to measure the altered behavior of the temperatures in the vicinity of the bubble due to the fluctuations caused by the bubble formation. With this idea of how to process we obtained a series of results for both the thermocouple and the microthermocouple.

4.4.1 Bubble life cycle analysis with regular K-type thermocouple

In order to create the bubble, the heat flux was increased. This was achieved by increasing the voltage and current. Specifically, the voltage and current values for this experiment were 1.08 V and 25.2 A, respectively. With these values and applying the Joule heat flux equation, a heat flux on the heated surface of about 15 kW/m^2 could be established. In addition, for the formation of the bubble at a certain point on the heated surface, a laser surface treatment was carried out and FDPA coating was applied to the surface, to give this point of the surface a certain hydrophobicity. This created well defined nucleation site that repeatedly provided similar bubble dynamics.

The temperature T_{bulk} = 95ºC had been established by preheating the water. Then, the distance of the thermocouple from the subsequently heated surface was measured. This measurement was carried out with the MATLAB software, as described in previous sections. Different temperature measurements were carried out at the heights shown in Table 4.8.

Table 4.8: Results of the heights determinations for the bubble experiment with the thermocouple.

Measurement	Height (mm)
1	4.40
2	2.20
3	1.30
4	0.40
5	~0.05

It should be noted that, as in the TBL experiment, the last measurement shows a distance to the heated surface of around 50 μm. This is because the smallest distance is determined relatively inaccurately.

Once the distance to the surface was determined, temperature measurements were made over time for each run. As in the TBL experiment, all temperatures at the beginning of the measurements (T_{bulk}) were not completely identical, so they were normalized following the procedure dictated above. Following this procedure, it can be observed not only that, as the thermocouple approaches the heated surface, the temperature variations are larger given the thermal boundary layer, but also, as the thermocouple gets closer to the triple contact line between the heated surface, the hot liquid and the vapor inside the bubble, the temperature fluctuations become larger and larger. Particularly at a distance of about 50 μm, temperature variations of up to 12.5°C, i.e. temperatures of 107°C, can be observed, as Figure 4.18 shows.

During the formation and growth of the bubble, a lot of energy is used in the form of heat absorption. The hot liquid surrounding the bubble near the nucleation point evaporates to contribute to the bubble growth. Due to mass continuity, the cold liquid, far from the nucleation point, replaces the evaporated hot liquid. This is why a drastic decrease in temperature is detected as the bubble is approached. Figure 4.19 shows a sketch of the proposed effect. On the other hand, specifically at the distance of 50 μm, the life cycle of the bubble can be explained step by step as named in the theoretical development section in Figure 2.9. First, there is a temperature increase as the water around the nucleated bubble absorbs the heat emitted by the heated surface. Subsequently, a radical decrease occurs as the bubble grows because the hot water around the bubble evaporates for the bubble to grow and is replaced by lower temperature water from the surroundings. Finally, the bubble departures from the surface at the temperature at which the next cycle of the next bubble begins.

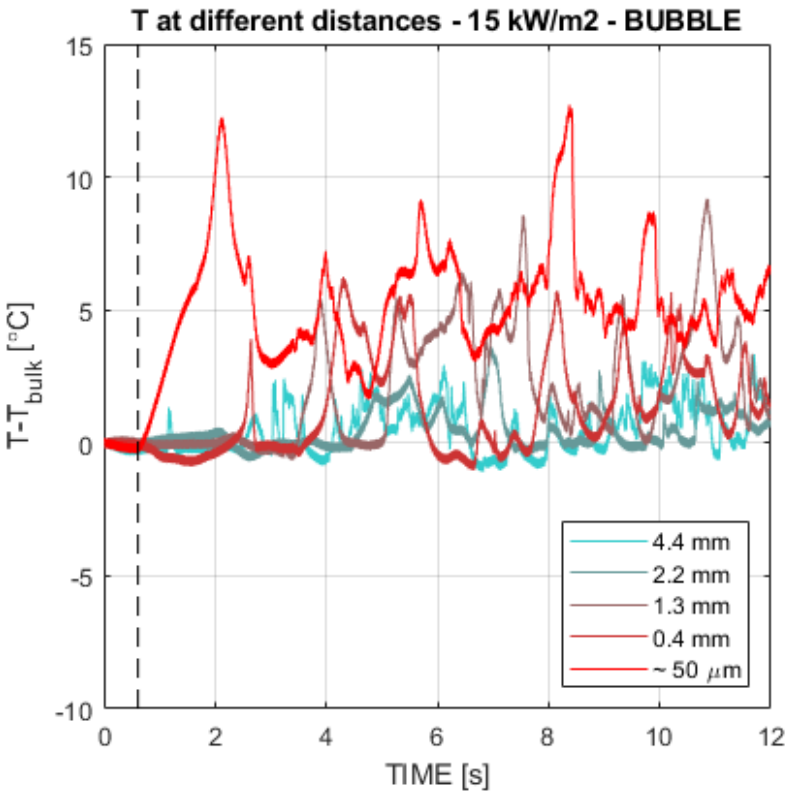

Figure 4.18: Normalized temperature at different heights from the heated surface in the thermocouple bubble experiment.

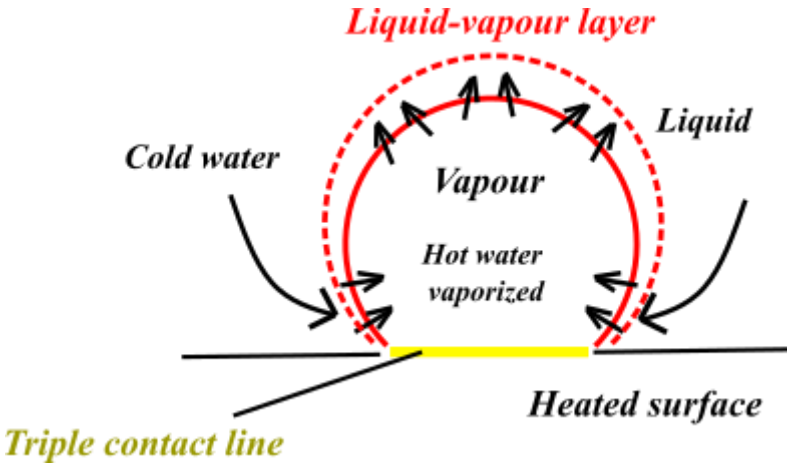

Figure 4.19: Procedure of bubble growth where the cold water substitutes the hot water evaporated in the bubble surroundings.

4.4.1.1 Bubble life cycle analysis with K-type microthermocouple

For the life cycle analysis of the bubble with the microthermocouple, the same steps were carried out as with the standard thermocouple. The bubble is formed thanks to the laser treatment of a part of the surface and the increase of the heat flux up to about 30 kW/m^2. For

this increase, it was only necessary to rise the voltage value to 2.2 V and the current value to 23.1 A. Subsequently, T_{bulk} was set to approximately 93°C for each measurement of the temperature variation by preheating the water. Different distances of microthermocouple position can be read in Table 4.9.

Table 4.9: Results of the heights determinations for the bubble experiment with the microthermocouple.

Measurement	Height (mm)
1	3.10
2	1.90
3	1.20
4	0.50
5	~0.02

It should be noted that, as in the TBL experiment, the last measurement shows a distance to the heated surface of around 20 μm and is relatively inaccurate.

Having determined these distances, the experiments for the analysis of the life cycle of a bubble are carried out. For each height, a series of temperature measurements regard to time were made as in the previous cases. Having obtained the results, they are normalised since not all the series of measurements started with the same initial temperature T_{bulk}. With these values normalised, it is represented in Figure 4.20 how the temperature varies as a function of time and certain distance from the heated surface.

As in the case of the thermocouple, as the microthermocouple approaches the heated surface while the bubble couples with its nucleation, growth and departure cycle, the temperature regard to T_{bulk} increases, as can be seen in the increasing values of temperature versus distance in Figure 4.20. In addition, when the microthermpole approaches the triple contact line, the fluctuations in the liquid increase as the cold water around the bubble replaces the hot water that evaporates to contribute to the bubble growth. This causes the temperature to vary drastically. Since the TBL is found at a height of about 20 μm, the sharpest temperature variations, up to 23ºC of difference, occurs at this height. In this position there is water at high temperature values of around 115ºC, which evaporates and is replaced by water at a much lower temperature, such as 100ºC, as seen in Figure 4.20 at timestamp of 2.8 seconds.

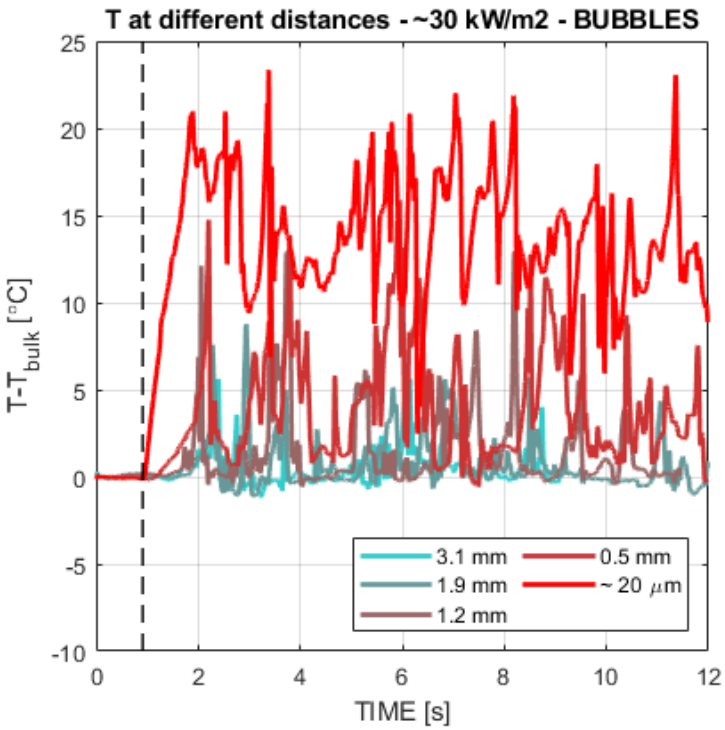

Figure 4.20: Normalized temperature at different heights from the heated surface in the microthermocouple bubble experiment.

It is important to note that the maximum temperature values in this experiment are in the order of 110 to 115°C, which is much higher than the T_{bulk}. This is due to the TBL, which is at a high temperature because the heat flux is much higher than the applied in the previous experiments. The aim of increasing the heat flux in this experiment was to be able to visualise more clearly how the microthermocouple behaves in the face of the most drastic temperature variations, observing that it has a fairly fast response, in the order of a few milliseconds. In fact, this is also the required time constant to capture these temperatures, as can be seen in the measurements in Figure 4.20.

The bubble life cycle can be explained as done previously, looking at the Figure 4.20. Firstly, the temperature increases as the water around the nucleated bubble absorbs the heat emitted by the heated surface. After that, the temperature radically decreases when the bubble grows. This is because the bubble is able to grow due to the hot water evaporating around the bubble. This hot water evaporated is replaced by lower temperature water. At the end, the bubble departures from the surface and cycle repeats again.

Other than discrete in-liquid temperature measurements performed with the micro-thermocouple approach, the transient thermal distribution of the boiling surface is essential to perform comprehensive boiling investigations. For this purpose, an infrared camera was used for both the thermocouple and the micro-thermocouple in the bubble life cycle analysis experiment. With this it is verified and understood how the thermal distribution varies along the heated surface and the liquid. This infrared camera captures the temperature of the heated surface during the nucleation, growth and departure of the bubble, as shown in Figure 4.21. It should be added that the temperature of the heated liquid very close to the surface does not differ much with regard to the heated surface temperature. In particular, our experiments

show they have a maximum difference of 1ºC. Therefore, the temperature of the fluid close to the surface can also be verified.

Another approach to understand the bubble life cycle is by analyzing the results of local temperature and heat flux transient fields. As explained earlier, the energy necessary for bubble nucleation was obtained by ohmic dissipation through the thin metal foil. When the desired voltage is applied to the electrodes, the foil starts to heat up as captured by the temperature and heat flux sequence reported in Figure 4.21. As the bubble nucleates (0 ms) and grows out from the nucleation site, a liquid microlayer forms underneath the bubble itself. Its evaporation is characterized by high heat flux values and provides a prompt local cooling of the boiling surface under the bubble of around 100 °C, which is the evaporating temperature. As the microlayer dries out, an actual dry patch forms and radially expands outwards from the nucleation site. Vapor has very low thermal conductivity, which explains why the local heat flux at the dry patch is close to 0 and its corresponding temperature keeps increasing in time, as seen during growth and departure (100–370 ms). At the same time, a high heat flux is measured around the triple contact line, due to local liquid evaporation. This is captured by the highly evaporating ring observed from 100 ms to until the departure (370 ms).

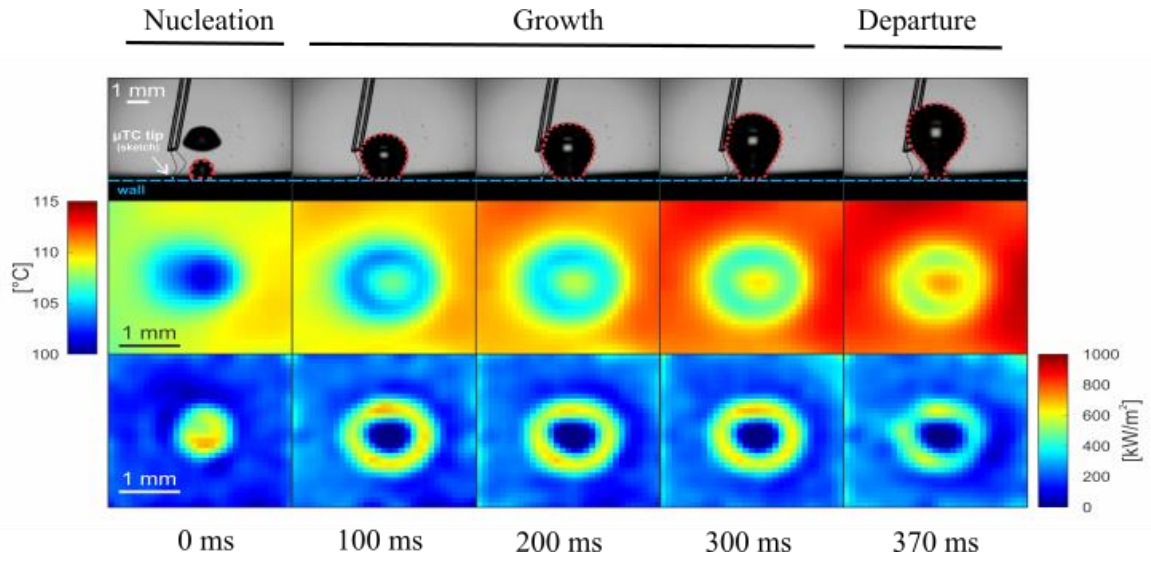

Figure 4.21: Temperature and heat flux captured by the infrared camera during the bubble life cycle for the microthermocouple bubble experiment.

To conclude, if the microthermocouple is compared to the thermocouple in this experiment, as it has been done in previous experiments, two conclusions can be drawn regarding the advantages of the former over the latter. The first is the greater accuracy of the MTC in measuring different local temperatures during the life cycle of a bubble. This is because the tip of the MTC is smaller than the one from the thermocouple, which allows us to get closer to positions that is more complicated to access, such as the triple contact line, and to take more precise and uniform measurements at a given location. The second conclusion is the higher measurement speed during the dynamic nucleate boiling situation. As discussed in the dynamic test, the MTC performs better in dynamic situations, as is the case here. Although the thermocouple detects these temperature variations during the bubble nucleation, growth, and departure, it performs much slower compared to the MTC, as can

be seen if Figure 4.18 and Figure 4.20 are analyzed simultaneously. The MTC is able to detect sudden temperature changes at millisecond timescale with relatively low uncertainty, thanks to its small thermal capacity and high-end data acquisition. All in all, the microthermocouple even being long-known technology still allows an approach to further the understanding of nucleate boiling. The process, which is still gaining a lot of attention despite several decades of research.

5 Conclusions

The ability to accurately measure temperatures in nucleate boiling in spatial and temporal domain is essential to understand mechanisms that take place in that complex heat transfer phenomena. To minimize the gap regarding the current inability of measuring transient temperature fields in-liquid around the growing vapor bubbles, some experimental analysis with the thermocouple and microthermocouple have been made within this thesis. We have experimentally analyzed the differences between normal commercial K-type thermocouple and custom developed microthermocouple. Static calibration test and measurement of dynamics response was performed, which showed significant enhancement regarding thermal time constant of the fine-wire microthermocouple. Furthermore, developed methodology was implemented to existing nucleate boiling apparatus and microthermocouple was successfully used to capture temperature variations around the growing bubble as well as inside the vapor in early stages of bubble growth. Most important conclusions and obtained results are provided below:

- During calibration, we have accurately measured the Seebeck coefficient for both K-type thermocouple and microthermocouple, which are 40.8560 μV/°C and 40.6428 μV/°C respectively.
- It was showed that the microthermocouple has a significantly faster response regard to the thermocouple, namely 48.125 times faster, in a dynamic situation.
- By using 24-bit signa-delta converter in a single-channel data acquisition card with a maximum sampling rate of 20 kHz, we measured the temperature and heat flux near the heated surface determining the position of the thermal boundary layer at around 50-100 μm, and validating, as well as understanding, the various steps of the bubble life cycle in nucleate boiling according to the various results obtained.
- The obtained results show that the microthermocouples can have an effective response time below 1 ms, of course depending on the effective heat transfer coefficient at the wire tip, which is enough to measure the effects during bubble growth and departure stage. Spatial resolution of such measurements are in the order of the wire diameter (around 25 μm in our case). Even thinner wires are possible, but significantly harder to manipulate and position inside the boiling chamber.

We therefore showed that the microthermocouple outperforms the conventional thermocouple. The results support the microthermocouple's position as a more advanced and sophisticated technology for measuring temperatures during nucleated boiling, making it suitable for applications requiring high accuracy and fast response. In our case we achieved to manufacture microthermocouple with experimentally determined time constant of 0,8 ms and a thermocouple tip of about 20 μm and successfully demonstrated its usefulness in atmospheric boiling of water. For that reason, we can fully confirm our research hypothesis.

For future work, we suggest the use of microthermocouples or even arrays of microthermocouples for the analysis of bubble life cycle in different fluids, the investigation of materials and wettability effects on the bubble growth and resulting in-liquid temperatures manufacture and, most importantly, for the improvement in the fundamental understanding of nucleate boiling process. This is essential to further optimize boiling surfaces for enhanced operation indifferent applications.

Bibliography

[1] Daniel D. Pollock: *Thermocouples. Theory and Properties*. 1st Edition. 1991.

[2] M. Zupančič and P. Gregorčič: *Laser surface engineering for boiling heat transfer applications, in Materials with Extreme Wetting Properties: Methods and Emerging Industrial Applications*. Springer International Publishing, 2021, pp. 245–303. doi: 10.1007/978-3-030-59565-4_12.

[3] S. Gong and P. Cheng: *Lattice Boltzmann simulation of periodic bubble nucleation, growth and departure from a heated surface in pool boiling. Int J Heat Mass Transf*. vol. 64, (2013) pp. 122–132, doi: 10.1016/j.ijheatmasstransfer.2013.03.058.

[4] S.G. Bankoff: *Entrapment of Gas in the Spreading of a Liquid Over a Rough Surface*. 1958.

[5] H. J. Cho and E. N. Wang: *Bubble nucleation, growth, and departure: A new, dynamic understanding*. *Int J Heat Mass Transf*. vol. 145, Dec. 2019, doi: 10.1016/j.ijheatmasstransfer.2019.118803.

[6] M. G. Cooper, A. J. P Lloyd, and G. Cooper: *the microlayer in nucleate pool boiling.* Pergamon Press, 1969.

[7] Y. Koizumi, M. Monde, and Y. Takata: *Outline of Boiling Phenomena and Heat Transfer Characteristics*, in *Boiling: Research and Advances*. Elsevier, (2017). doi: 10.1016/B978-0-08-101010-5.00001-4.

[8] B. B. Mikic, W. M. Rohsenow, and P. Griff'ith: *on bubble growth rates*.

[9] M. S. Plesset and S. A. Zwick: *The growth of vapor bubbles in superheated liquids*, *J Appl Phys*. vol. 25, no. 4, (1954) pp. 493–500, doi: 10.1063/1.1721668.

[10] S. J. D Van Stralen, M. S. SoHAL, R. Cole, and W. M. Sluyter: *bubble growth rates in pure and binary systems: combined effect of relaxation and evaporation microlayers*. Pergamon Press, 1975.

[11] T. P. Allred, J. A. Weibel, and S. V. Garimella: *The Role of Dynamic Wetting Behavior during Bubble Growth and Departure from a Solid Surface*. *Int J Heat Mass Transf*. vol. 172, Jun. 2021, doi: 10.1016/j.ijheatmasstransfer.2021.121167.

[12] H. T. Phan, N. Caney, P. Marty, S. Colasson, and J. Gavillet: *How does surface wettability influence nucleate boiling? Comptes Rendus – Mecanique*. vol. 337, no. 5, (2009) pp. 251–259, doi: 10.1016/j.crme.2009.06.032.

[13] M. Buchholz, T. Lüttich, H. Auracher, and W. Marquardt: *Experimental investigation of local processes in pool boiling along the entire boiling curve*. *Int J Heat Fluid Flow*. vol. 25, no. 2, (Apr. 2004), pp. 243–261, doi: 10.1016/j.ijheatfluidflow.2003.11.020.

[14] A. Ono and H. Sakashita: *Temperature measurements near a heating surface at high heat fluxes in subcooled pool boiling*. *Heat Transfer - Asian Research*. vol. 39, no. 1, (Jan. 2010) pp. 27–42, doi: 10.1002/htj.20277.

[15] T. Yabuki, T. Hamaguchi, and O. Nakabeppu: *Interferometric measurement of the liquid-phase temperature field around an isolated boiling bubble*. Journal of Thermal Science and Technology. vol. 7, no. 3, (2012) pp. 463–474, doi: 10.1299/jtst.7.463.

[16] S. Narayan, A. Srivastava, and S. Singh: *Rainbow schlieren-based investigation of heat transfer mechanisms during isolated nucleate pool boiling phenomenon: Effect of superheat levels. Int J Heat Mass Transf*. vol. 120, (May 2018) pp. 127–143, doi: 10.1016/j.ijheatmasstransfer.2017.12.005.

[17] V. Voulgaropoulos, G. M. Aguiar, C. N. Markides, and M. Bucci: *Simultaneous laser-induced fluorescence, particle image velocimetry and infrared thermography for the investigation of the flow and heat transfer characteristics of nucleating vapour bubbles. Int J Heat Mass Transf*. vol. 187, May 2022, doi: 10.1016/j.ijheatmasstransfer.2022.122525.

[18] T. Bregar, M. Vodopivec, T. Pečnik, M. Zupančič, and I. Golobič: *Pool-Boiling Performance on Thin Metal Foils with Graphene-Oxide-Nanoflake Deposit, Nanomaterials*. vol. 12, no. 16, Aug. 2022, doi: 10.3390/nano12162772.

[19] P. Gregorčič, M. Zupančič, and I. Golobič: *Scalable Surface Microstructuring by a Fiber Laser for Controlled Nucleate Boiling Performance of High- and Low-Surface-Tension Fluids.* Sci Rep. vol. 8, no. 1, Dec. 2018, doi: 10.1038/s41598-018-25843-5.